CHALMERS
UNIVERSITY OF TECHNOLOGY

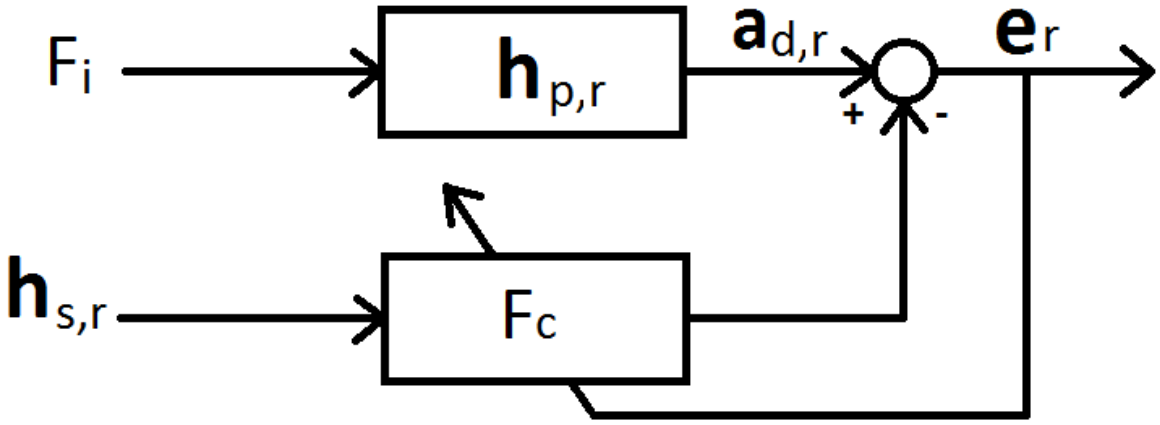

Active Control of Impact Noise

A study on the reduction of the radiated sound power resulting from an impact between a sphere and a plate

Master of Science Thesis in the Master's Programme Sound and Vibration

ANDRÉ VINÍCIUS VIACAVA PASSANESI

Department of Civil and Environmental Engineering
Department of Applied Acoustics
Vibroacoustics Research Group
CHALMERS UNIVERSITY OF TECHNOLOGY
Gothenburg, Sweden 2017
BOMX02-2016-129

BOMX02-2016-129

Active Control of Impact Noise

A study on the reduction of the radiated sound power resulting from an impact between a sphere and a plate

Master of Science Thesis in the Master's Programme Sound and Vibration

ANDRÉ VINÍCIUS VIACAVA PASSANESI

CHALMERS
UNIVERSITY OF TECHNOLOGY

Department of Civil and Environmental Engineering
Division of Applied Acoustics
Vibroacoustics Research Group
Chalmers University of Technology
Gothenburg, Sweden 2017

Active Control of Impact Noise
A study on the reduction of the radiated sound power resulting from an impact between a sphere and a plate
Master of Science Thesis in the Master's Programme Sound and Vibration
ANDRÉ VINÍCIUS VIACAVA PASSANESI

BOMX02-2016-129
Department of Civil and Environmental Engineering
Division of Applied Acoustics
Vibroacoustics Research Group
Chalmers University of Technology
SE-412 96 Gothenburg
Telephone +46 31 772 1000

Cover: Sketch of the modified LMS-algorithm developed for and used in this work.

Typeset in LaTeX
Printed by Chalmers Reproservice
Gothenburg, Sweden 2017

Active Control of Impact Noise
A study on the reduction of the radiated sound power resulting from an impact between a sphere and a plate
Master of Science Thesis in the Master's Programme Sound and Vibration
ANDRÉ VINÍCIUS VIACAVA PASSANESI
Department of Civil and Environmental Engineering
Division of Applied Acoustics
Vibroacoustics Research Group
Chalmers University of Technology

Abstract

Impacts are an important noise source of today's society. From a control standpoint, solutions to problems related to impacts are commonly based on passive methods. In this paper, an active method to control the radiated sound from a sphere impacting a simply supported plate attached to an infinite baffle is proposed. The contact force between sphere and plate is modeled by Hertzian contact, this force is then convoluted with the plate's impulse response. From this, the radiated sound field is calculated by the Rayleigh integral in the time domain. In a following step, an active force is used to act on the plate with the purpose of minimizing the radiated sound power. This control force is estimated using a method based on the LMS algorithm formulated in the time-domain. For different positions of the impact between the sphere and the plate, the position of the active force is varied and for each case, the LMS algorithm obtains the optimal time record of the force. For non-trivial cases, where the acting force is not in the same position as the impact, results present reductions of up to 13 dB in the simulations of the radiated sound power.

Keywords: Active vibration control, impact control, sound radiation.

Acknowledgements

I would like to acknowledge my supervisor and mentor, Wolfgang Kropp, whose help and guidance was fundamental for the completion of this work. I also would like to thank Carsten Hoever and Lars Hansson for their technical support throughout the development of this thesis. Another big thanks goes to my mother and my father, Nilde and Hamilton Passanesi, my siblings, Thaís and Eduardo Passanesi, and my girlfriend, Patrícia Belletati, who always believed in me and gave me all the moral support I needed besides helping me keep a calm and focused mind to achieve my goals.

This work has been produced during my scholarship period at Chalmers University of Technology, thanks to a Swedish Institute scholarship. Without their financial support, this work as well as the past two years of education which the author received would not be possible.

André Vinícius Viacava Passanesi, Gothenburg, August 2016.

Contents

List of Figures **xi**

List of Tables **xiii**

1 Introduction **1**

2 Theory **3**
2.1 Sound Radiation from Impacts 3
2.1.1 Formulation of the equations to find the impact force 4
2.1.2 Numerical methods applied to calculate the impact force . . . 6
2.1.3 Plate impulse response 10
2.1.4 Radiated sound 11
2.2 Active Noise Control 13
2.2.1 The Least Mean Square algorithm 13
2.2.2 Force identification method based on LMS algorithm 15
2.2.3 Multidegree of freedom LMS 16

3 Simulation setup and results **19**
3.1 Definition of plate and sphere to be studied 19
3.2 Initial conditions and defined calculation parameters 20
3.3 Determination of the input forces 21
3.4 Frequency study 24

4 LMS Algorithm **27**
4.1 Decription of the applied LMS algorithm 27
4.2 Results for impact position 1 29
4.3 Results for impact position 2 35
4.4 Results for impact position 3 40

5 Radiated sound power evaluation **45**

6 Conclusion **47**
6.1 Future work 47

Bibliography **49**

List of Figures

2.1 Schematic depiction of the studied plate and sphere. 4
2.2 Depiction of the relative displacement between sphere and plate. . . . 5
2.3 Flowchart representing the process to calculate the impact force taken from [3]. 9
2.4 Block diagram of an adaptive filter taken from [16]. 13
2.5 Sketch of how the LMS algorithm is applied in this work. 15
2.6 Sketch of the LMS algorithm used in this work after the necessary alterations 17

3.1 Schematic depiction of the studied plate with dimensions. 19
3.2 Schematic depiction of the studied sphere with dimensions. 20
3.3 Sketch of the simply supported plate and the different impact positions that were simulated 22
3.4 Impact forces for different impact positions 22
3.5 Viscous forces for different impact positions 23
3.6 Frequency domain representation of total input force 24
3.7 Radiation efficiency of the studied plate. The solid blue line represents the efficiency achieved from modal superposition and the dotted black lines are the efficiencies of the first 15 modes separately. 25

4.1 Example of the resampled total force used as an input to the LMS algorithm. 27
4.2 Example transfer function for a specific receiving position. 28
4.3 Example of the primary path for the same position as shown previously. 29
4.4 Results obtained from the simulation of an impact applied in position 1 with an active force applied in control position 1. 30
4.5 Results obtained from the simulation of an impact applied in position 1 with an active force applied in control position 2. 31
4.6 Results obtained from the simulation of an impact applied in position 1 with an active force applied in control position 3. 32
4.7 Results obtained from the simulation of an impact applied in position 1 with an active force applied in control position 4. 33
4.8 Results obtained from the simulation of an impact applied in position 2 with an active force applied in control position 1. 36
4.9 Results obtained from the simulation of an impact applied in position 2 with an active force applied in control position 2. 37

4.10 Results obtained from the simulation of an impact applied in position 2 with an active force applied in control position 3. 38
4.11 Results obtained from the simulation of an impact applied in position 2 with an active force applied in control position 4. 39
4.12 Results obtained from the simulation of an impact applied in position 3 with an active force applied in control position 1. 41
4.13 Results obtained from the simulation of an impact applied in position 3 with an active force applied in control position 2. 42
4.14 Results obtained from the simulation of an impact applied in position 3 with an active force applied in control position 3. 43
4.15 Results obtained from the simulation of an impact applied in position 3 with an active force applied in control position 4. 44

List of Tables

3.1 Overview of material properties 20
3.2 Impact position coordinates 21

5.1 Reduction in radiated sound power. The trivial solution reductions are in italic and the largest reductions found for a non-trivial impact position are in bold. 45

1
Introduction

Weather in residences or in the workplace, impacts are an important source of noise in today's society. The concern with this type of noise increases in industry due to the large presence of machinery whose mechanical processes include impacts [1]. Planing, pressing, stamping, forging and other hammer-type operations are some examples of such machines. Because of the materials involved, the sound pressure levels resulting from these impacts can present a health risk, leading to a need of legislation [3]. However, given the transient nature and short duration of impact noise, the produced sound is difficult to control, culminating in a larger struggle to meet the emission regulations [4].

With the use of passive absorbers, it is possible to attenuate high frequencies in the radiated sound resulting from the impacts [5]. Nonetheless, this might lead to an obstruction of the access to the machine. Another concern with this type of solution is the impractical control of lower frequencies and vibrations. Thus, for an effective result in the attenuation of all frequencies, actions must be taken at the source level [6]. When dealing with impacts, this source level is the contact between the colliding bodies, meaning that by controlling the way this collision occurs, it is possible to control all the subsequent outcomes of the impact. For this, active control can be of great value.

The concept of active control applied in this research is the use of electroacoustic transducers to modify/control sound fields. To simplify this rather broad topic of impacts, a sphere impacting on a plate which is simply supported by an infinite baffle was selected as the generic study case. An artificial active point force applied to the plate is the chosen actuation method. The aim of this thesis is to investigate possible active control measures with the purpose of reducing the radiated sound resulting from such an impact. Although this setup does not cover many of the features present in the aforementioned industrial machinery, it is considered sufficient as a theoretical setup to be used as a first step for more complex constructions. This is a necessary provision, given that there is a rather small amount of literature on the use of active control for impact problems, especially from an acoustic point of view.

This report is written in the following way: chapter 2 introduces the fundamental theory necessary for the development of this work; chapter 3 presents the simulation setup used in this work along with the necessary initial calculations and results which are used as an input to the main algorithm used in this work; chapter 4 shows

this main algorithm as well as the results obtained from it and a discussion on these results; chapter 6 contains an analysis on the changes on radiated sound power resulting from the results obtained in chapter 5; chapter 7 presents the conclusions from this work and suggestions for future investigations.

2
Theory

The physical phenomena and equations relevant to this work will be presented and discussed in the following chapter. The models chosen as well as the simplifications utilized and the limitations of these will also be exposed.

2.1 Sound Radiation from Impacts

An impact is defined as a high force applied on colliding bodies during a short period of time [7]. During this collision, a complex process occurs where minute changes to the contact conditions between the two bodies can greatly influence the outcome of this impact. One of the key characteristics of this mechanical phenomenon is the transformation of kinetic energy into potential energy in the form of elastic deformations and subsequently to heat and sound energy, the latter being of main interest for this work.

In a broad perspective, the energy that is converted into sound energy during an impact, and thus perceived as noise, can be subdivided into two main categories: the acceleration noise and the ringing noise [8]. The acceleration noise is the noise component caused by pressure perturbations due to the sudden deceleration and acceleration of the sphere at impact. The ringing noise is the noise component due to the sound radiation from the vibrations of the structure in which the impact occurred. In this thesis work, the focus was kept in the ringing noise component of the impact sound, and thus only this component will be explored in the following theoretical depiction of this problem.

Due to the presence of a control force in the studied system, the impact cannot be described with the equations commonly used for collisions. Thus, a more primitive approach to these impact equations, which relies on the equations of motion of the impacting objects, must be followed to describe the problem at hand. The theoretical formulation presented in [1] does this and it is based on three necessary calculation steps to find the radiated sound emitted for the case studied. These steps are: the calculation of the impact force, the response of the plate to this load and, lastly, the finding of the acoustic pressure at any point in space. Each of these calculation steps will be described next in further detail.

The studied sphere and simply supported plate that comprise the case studied are depicted in figure 2.1 and all equations will be presented in accordance to the coor-

dinate system presented in this figure.

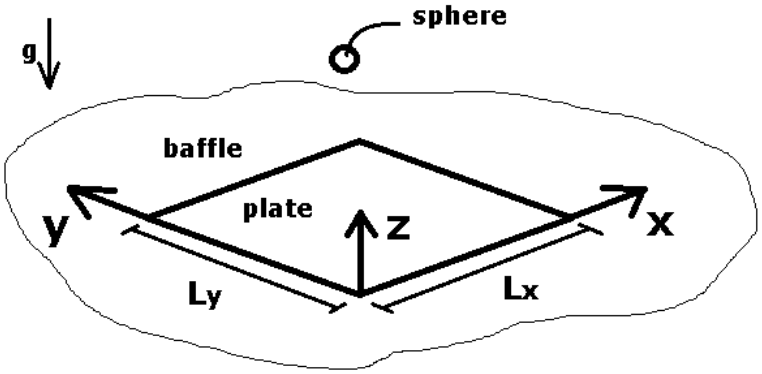

Figure 2.1: Schematic depiction of the studied plate and sphere.

2.1.1 Formulation of the equations to find the impact force

Assuming the impact between the sphere and the plate is elastic, it is possible to estimate the contact force through Hertz's theory for contact stress [7]. On doing so, the deformations that occur during the impact, which lead to a varying contact area between the plate and sphere, are considered. Hertz's theory presents a non-linear relation between the contact and the force, expressed by:

$$F_c(t) = s\xi(t)^{\frac{3}{2}} \tag{2.1}$$

where F_c is the contact force, ξ is the relative displacement between the ball and plate and s is the contact stiffness, which is represented by:

$$s = \frac{4}{3}\sqrt{r_s}\left[\frac{1-\nu_s^2}{E_s} + \frac{1-\nu_p^2}{E_p}\right]^{-1} \tag{2.2}$$

where r_s is the radius of the sphere, ν and E are respectively the Poisson's ratios and Young's modulus associated with each body, represented with the subscript s for sphere and p for plate.

Besides the assumption of an elastic collision, there are several other suppositions related to this theory. First, the bodies in contact should be considered elastic half-spaces. Also, the strains in the contact must be small and stay within the elastic limit. This leads to the implication that the contact surfaces in question are much smaller than the characteristic dimensions of the bodies involved in the collision. Lastly, the surface should be friction-less, which implies that the plate and sphere have similar elastic properties [3].

Limits to these assumptions are, for example, impacts between bodies of soft materials or impacts with a high velocity. Such cases will not be evaluated in this work. It is also important to note that this force is only applied while there is contact between the sphere and plate, and therefore, only when the relative displacement

between the two is smaller than zero. This relative displacement is illustrated in figure 2.2 and expressed as:

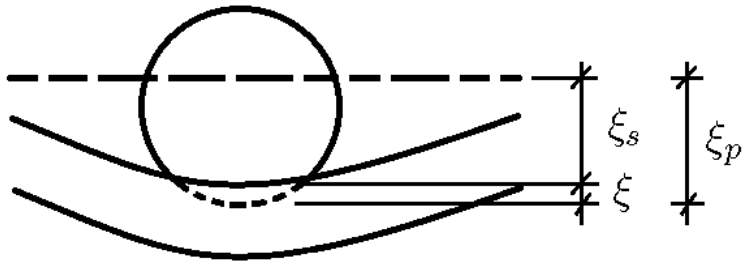

Figure 2.2: Depiction of the relative displacement between sphere and plate.

$$\xi(t) = \xi_s(t) - \xi_p(t) \tag{2.3a}$$

deriving this twice in relation to time:

$$\ddot{\xi}(t) = \ddot{\xi}_s(t) - \ddot{\xi}_p(t) \tag{2.3b}$$

where ξ_s is the position of the bottommost point of the sphere and ξ_p is the position of the top side of the plate. Therefore, the equations for the displacement of the sphere and the plate are necessary. Once contact is made, the contact force is applied on both the plate and sphere. Thus, the equation of movement for the sphere will be:

$$m_s\ddot{\xi}_s = -F_c - m_s g \tag{2.4}$$

where m_s is the mass of the sphere and g is the gravity. Note that the negative sign for the contact force is due to the reference being used (where this force only exists for $\xi \leq 0$).

One can express the position of a certain point of the plate as a convolution between the forces acting on the plate and the impulse response of the plate. In the case studied, the acting forces are the contact force and the controlled active force, rendering the following equation:

$$\xi_p(t) = F_a(t) * M_a(t) + F_c(t) * M_c(t) \tag{2.5a}$$

or

$$\xi_p(t) = \int_0^t F_a(\tau)M_a(t-\tau)d\tau + \int_0^t F_c(\tau)M_c(t-\tau)d\tau \tag{2.5b}$$

where ξ_p is the displacement of a point in the plate, F_c and F_a are the contact and active forces respectively, and M_c and M_a are the impulses responses corresponding to the position of the plate where the contact and active forces are applied. These impulse responses will be exposed and discussed later on. For now, it is sufficient

to state that they naturally do not depend on any displacement. Deriving equation 2.5b twice in terms of time leads to:

$$\ddot{\xi}_p(t) = \int_0^t F_a(\tau)\ddot{M}_a(t-\tau)d\tau + \int_0^t F_c(\tau)\ddot{M}_c(t-\tau)d\tau \tag{2.6}$$

Inserting equations 2.3b, 2.1 and 2.6 into 2.4 results in:

$$m_s\left[\int_0^t F_a(\tau)\ddot{M}_a(t-\tau)d\tau + \int_0^t s\xi(\tau)^{\frac{3}{2}}\ddot{M}_c(t-\tau)d\tau + \ddot{\xi}(t) + g\right] + s\xi(t)^{\frac{3}{2}} = 0 \tag{2.7}$$

Equation 2.7, if solved, yields the behaviour of the relative displacemente, ξ, which would subsequently give the impact force through equation 2.1. However, it is very difficult to solve a non-linear ordinary differential equation analytically. On that account, a discretization of time as well as the use of numerical methods was adopted to reach the desired solution. These will be exposed and discussed in the next section, but before this, damping will be introduced to the equations above.

For simplicity, only viscous damping will be evaluated in this work. Other approaches can be found in [3]. The formulation used for viscous damping in this work is a linear model expressed as:

$$F_v(t) = c \cdot \dot{\xi}(t) \tag{2.8}$$

where c is the viscous damping factor. This factor is obtained through an initial estimation followed by further adjustments to reach the appropriate level of damping. The viscous force is applied to the point of contact and must be thus added to equations 2.4 and 2.6, which leads to the following change in equation 2.7:

$$m_s\left[\int_0^t F_a(\tau)\ddot{M}_a(t-\tau)d\tau + \int_0^t (s\xi(\tau)^{\frac{3}{2}} + c\dot{\xi}(\tau))\ddot{M}_c(t-\tau)d\tau + \ddot{\xi}(t) + g\right] + s\xi(t)^{\frac{3}{2}} + c\dot{\xi}(t) = 0 \tag{2.9}$$

2.1.2 Numerical methods applied to calculate the impact force

First, in order to apply the desired numerical approach, it is necessary to discretize time. This means that the variable time will no longer be continuous, which leads to the need of certain changes in the mathematical representation presented earlier. One important aspect of the sampling that will be performed is that errors will arise from it. However, the short duration of the impact imposes the requirement of a high sampling rate, lowering the amount of noise generated from this process.

To evaluate equation 2.9 in a discrete space, it is necessary to express the convolutions in this equation in a discrete form. These mathematical operations are expressed in the following form in a discrete space [10]:

$$(f * g)(t_N) = \Delta t \sum_{i=1}^{N} f(t_i) g(t_{N-i+1}) \tag{2.10}$$

where f and g are the discrete functions being convoluted, Δt is the time step and the subscript N represents the current time step. Applying this to the convolution between the contact force and the impulse response function of the plate, the following equation is obtained.

$$(F_c * \ddot{M}_c)(t_N) = \Delta t \sum_{i=1}^{N} s\xi(t_i)^{\frac{3}{2}} \ddot{M}_c(t_{N-i+1}) \tag{2.11}$$

Equation 2.11 indicates the need of full knowledge of the variable ξ up to the current time step. However, this is the exact variable which the equation is being solved for. Thus, it is interesting to perform a mathematical step to isolate the current step in the equation, yielding the following result.

$$(F_c * \ddot{M}_c)(t_N) = \Delta t(s\xi(t_N)^{\frac{3}{2}})\ddot{M}_c(t_1) + \Delta t \sum_{i=1}^{N-1} s(\xi(t_i)^{\frac{3}{2}})\ddot{M}_c(t_{N-i+1}) \tag{2.12}$$

The process is analogous for both the active force and the viscous force, however it is not necessary to isolate the current time step in the case of the active force. This is because the displacement is not involve in that particular convolution. Substituting these convolutions into equation 2.9, as well as using discrete time, leads to:

$$\begin{aligned} m_s\Bigg(&\Delta t(s\xi(t_N)^{\frac{3}{2}} + c\dot{\xi}(t_N))\ddot{M}_c(t_1) + \Delta t \sum_{i=1}^{N-1}(s\xi(t_i)^{\frac{3}{2}} + c\dot{\xi}(t_i))\ddot{M}_c(t_{N-i+1}) + ... \\ &+ \Delta t \sum_{i=1}^{N} F_a(t_i)^{\frac{3}{2}} \ddot{M}_a(t_{N-i+1}) + \ddot{\xi}(t_N) + g\Bigg) + s\xi(t_N)^{\frac{3}{2}} + c\dot{\xi}(t_N) = 0 \end{aligned} \tag{2.13}$$

where t_N is the current time step and t_1 is the first time step. Even though equation 2.13 is rather large, it is only dependent of three unknown variables: ξ, $\dot{\xi}$ and $\ddot{\xi}$. Thus, a numerical method that relates these three is needed to solve this equation.

The numerical method chosen to correlate these variables is the Hilber-Hughes-Taylor method (HHT). HHT is an implicit method, which in this case means it finds a solution for equations involving both the current time step and the previous ones [11]. This method also allows for numerical damping without lowering order accuracy. This is done with the use of a parameter referred to as the α. Through the use of this, the equations for the relative displacement and velocity become:

$$\xi_{HHT}(t_N) = \xi(t_{N-1}) - \alpha\Delta t\dot{\xi}(t_{N-1}) - \alpha\Delta t^2\left[\left(\frac{1}{2} - \beta\right)\ddot{\xi}(t_{N-1}) + \beta\ddot{\xi}(t_N)\right] \tag{2.14a}$$

$$\dot{\xi}_{HHT}(t_N) = \dot{\xi}(t_{N-1}) - \alpha\Delta t[(1-\gamma)\ddot{\xi}(t_{N-1}) + \gamma\ddot{\xi}(t_N)] \tag{2.14b}$$

where β and γ are functions of α, expressed as:

$$\beta = \frac{(1-\alpha)^2}{4} \tag{2.15a}$$

$$\gamma = \frac{1-2\alpha}{2} \tag{2.15b}$$

The parameter α determines the amount of numerical damping utilized and should therefore be kept within the interval $[-\frac{1}{3}, 0]$. With these equations, there is now only one unknown variable left to solve for in equation 2.13, the relative acceleration $\ddot{\xi}$. For this, the Newton-Raphson method was selected.

The Newton-Raphson method is a numerical method utilized to solve for the roots of a certain equation, parting from an initial approximation of this root [12]. It is expressed by the following equation:

$$x_n = x_{n-1} - \frac{f(x_{n-1})}{f'(x_{n-1})} \tag{2.16}$$

where x is the variable which the method solves for, n is the n-th iteration, f is the equation in question and f' is the derivative of this equation in terms of the variable studied. Equation 2.16 must be repeated until the error between the result of two consecutive iterations is below a determined tolerance level. Note that the N in equation 2.13 and the n in equation 2.16 are different, as first pertains to the current time step and the latter to the current iteration.

For the case at hand, the variable x is the relative acceleration $\ddot{\xi}$ and the function f is equation 2.13 with equation 2.14a. The derivative of this resulting equation in terms of the relative acceleration results in:

$$\frac{\partial f}{\partial \ddot{\xi}(t_N)} = m_s + \frac{3}{2}\frac{\partial \xi(t_N)}{\partial \ddot{\xi}(t_N)}\xi(t_N)^{\frac{1}{2}}(m_s s \Delta t \ddot{M}_c(t_1) + s) + \frac{\partial \dot{\xi}(t_N)}{\partial \ddot{\xi}(t_N)}(m_s c \Delta t \ddot{M}_c(t_1) + c) \tag{2.17}$$

where the differential is equal to:

$$\frac{\partial \xi(t_N)}{\partial \ddot{\xi}(t_N)} = -\alpha \Delta t^2 \beta \tag{2.18a}$$

$$\frac{\partial \dot{\xi}(t_N)}{\partial \ddot{\xi}(t_N)} = -\alpha \Delta t \gamma \tag{2.18b}$$

With this, all the necessary equations and methods to find the impact force have been described. As the input to the process, the free fall equations are used, where:

$$\dot{\xi}_0 = -\sqrt{2g(\xi_{s,0} - \xi_{p,0})} \tag{2.19a}$$

$$\ddot{\xi}_0 = -g \tag{2.19b}$$

where $\xi_{s,0}$ and $\xi_{p,0}$ are the initial positions of the sphere and plate respectively. Once contact is made, the Newton-Raphson method is used to find the relative acceleration of the current step. It is repeated until the error between iterations is lower than the tolerance. Then, with the use of the HHT equations, the relative velocity and position are calculated. This process is repeated $\xi \leq 0$. Figure 2.3 illustrates this process in a flowchart [3].

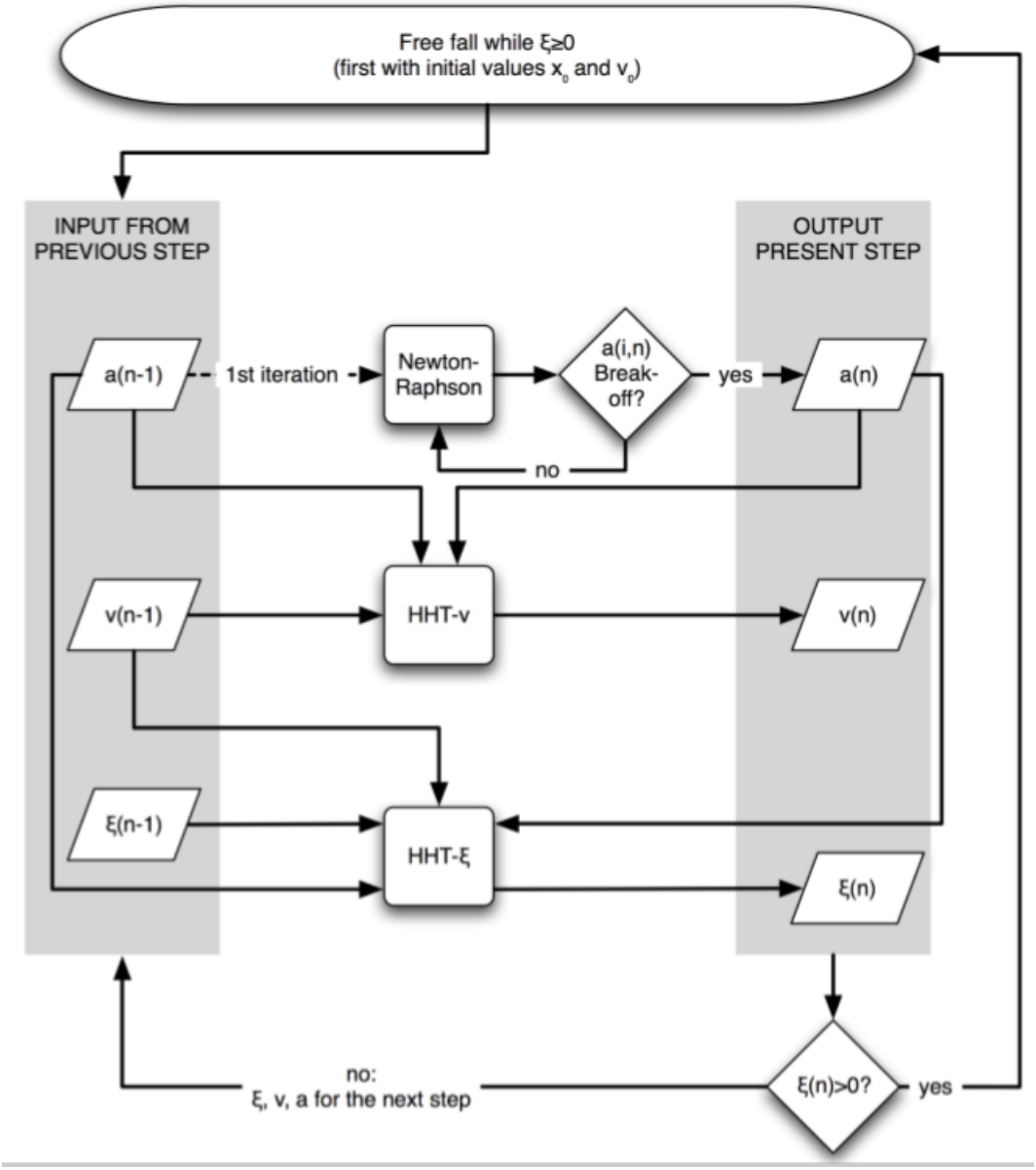

Figure 2.3: Flowchart representing the process to calculate the impact force taken from [3].

With knowledge of how ξ behaves, the contact force can be calculated. Therefore, the excitation characteristics have been determined and now a study of the response of the plate is needed.

2.1.3 Plate impulse response

An impulse response characterizes how a certain system reacts to any external input. The concept behind this relies on using a short pulse as an input to the system and verifying the resulting output from this same system. This response has been well characterized for a simply supported plate in both the time and frequency domains. Since the earlier sections in this report only used the time domain, only the equations pertaining to it will be exposed here.

An impulse response of the displacement of a plate can be calculated through the sum of all it's eigenfunctions, expressed as [5]:

$$M(x,y,t) = -\frac{4}{m_p}\sum_{n=1}^{\infty}\sum_{m=1}^{\infty}\Phi_e(x_e,y_e,n,m)\Phi_r(x_r,y_r,n,m)\frac{\sin(\Theta_{n,m}t)}{\Theta_{n,m}}e^{-\delta_{n,m}t} \quad (2.20)$$

where m_p is the mass of the plate, n and m are integers that represent the eigenfunctions in the x and y directions respectively, Φ_e and Φ_r are the eigenfunctions at the excitation point and a receiving point withing the plate respectively, (x_e, y_e) and (x_r, y_r) are the positions of these points, and $\Theta_{n,m}$ and $\delta_{n,m}$ are functions of the eigenfrequencies of the plate with added damping, given by:

$$\Theta_{n,m} = \omega_{n,m}\sqrt{1-\frac{\eta^2}{4}} \quad (2.21a)$$

$$\delta_{n,m} = \frac{\eta}{2}\omega_{n,m} \quad (2.21b)$$

where $\omega_{n,m}$ are the eigenfrequencies of the plate and η is the damping coefficient.

For the case of a simply supported case, the eigenfrequencies and eigenfunctions of the plate can be described mathematically in a very simple manner [1]. This is why this case was chosen for this thesis work. The eigenfunctions are expressed as follows:

$$\Phi_{n,m,i} = \sin\left(\frac{n\pi x_i}{L_x}\right)\sin\left(\frac{m\pi y_i}{L_y}\right) \quad (2.22)$$

where L_x and L_y are the lengths of the plate in the x and y directions respectively, and the index i represents either the excitation or receiving points. The eigenfrequencies are written as:

$$\omega_{n,m} = \sqrt{\frac{B'}{m''}}\left[\left(\frac{n\pi}{L_x}\right)^2 + \left(\frac{m\pi}{L_y}\right)^2\right] \quad (2.23)$$

where m'' is the mass per unit area of the plate, calculated through $m'' = \rho h$, where ρ is the plate density and h is the thickness. And B' is the bending stiffness of the plate, found through:

$$B' = \frac{E_p h^3}{12(1-\nu_p)} \quad (2.24)$$

where h is the thickness of the plate.

This is sufficient to verify the behaviour of the position of the points in the plate. But in equation 2.13, the response in terms of the acceleration is needed. To find this, equation 2.20 must be derived twice in terms of time. The result is:

$$\frac{\partial M}{\partial t} = -\frac{4}{m_p}\sum_{n=1}^{\infty}\sum_{m=1}^{\infty}\frac{\Phi_e\Phi_r}{\Theta_{n,m}}\Big(\cos(\Theta_{n,m}t)\Theta_{n,m}e^{-\delta_{n,m}t} - \sin(\Theta_{n,m}t)e^{-\delta_{n,m}t}\delta_{n,m}\Big) \tag{2.25a}$$

$$\frac{\partial^2 M}{\partial t^2} = -\frac{4}{m_p}\sum_{n=1}^{\infty}\sum_{m=1}^{\infty}\frac{\Phi_e\Phi_r}{\Theta_{n,m}}\Big[\Big(\delta_{n,m}^2 - \Theta_{n,m^2}\Big)\sin(\Theta_{n,m}t) - 2\Theta_{n,m}\delta_{n,m}\cos(\Theta_{n,m}t)\Big]e^{-\delta_{n,m}t} \tag{2.25b}$$

Expressing equation 2.25b for the contact point will only change the eigenfunctions involved in the equation. These will be:

For the contact and viscous forces

$$\Phi_e\Phi_r = \sin^2\left(\frac{n\pi x_c}{L_x}\right)\sin^2\left(\frac{m\pi y_c}{L_y}\right) \tag{2.26a}$$

For the active force

$$\Phi_e\Phi_r = \sin\left(\frac{n\pi x_c}{L_x}\right)\sin\left(\frac{m\pi y_c}{L_y}\right)\sin\left(\frac{n\pi x_a}{L_x}\right)\sin\left(\frac{m\pi y_a}{L_y}\right) \tag{2.26b}$$

where (x_c, y_c) and (x_a, y_a) are the points where the impact occurs and where the active force is applied respectively.

With the input described in the previous sections, it is possible to unite the exposed acceleration impulse responses with the forces through a convolution and verify the resulting behaviour of any point within the plate. This would then allow for the calculation of the radiated sound, which will be shown next.

2.1.4 Radiated sound

To determined the sound field generated by the impact, the Rayleigh integral was used. This technique is based on the idea that the radiating body can be constructed by the addition of infinitesimal monopole sources [13]. The Rayleigh integral which allows the calculation of the radiated pressure from an arbitrary vibration pattern on the baffled plate is:

$$p(R,t) = \frac{\rho_0}{2\pi}\int_S \frac{\ddot{\xi}(t, r_s)}{|R - r_s|}\,dS \tag{2.27}$$

where R is the position of the chosen receiving point, ρ_0 is the specific density of air, S is the area of integration which in this case is the plate, $\ddot{\xi}(t, r_s)$ is the acceleration of an arbitrary source point and r_s is the position of the arbitrary source within the

plate.

Since the calculation of the radiated pressure is done numerically, there is a need to discretize the plate in small elements and then sum their contributions. This will change equation 2.27 in the following way:

$$p(R,t) = \frac{\rho_0}{2\pi} \sum_{i=1}^{S/dxdy} \frac{\ddot{\xi}(t, r_{s,i})\, dx\, dy}{|R - r_{s,i}|} \tag{2.28}$$

where dx and dy are the discretization sizes in the x and y directions respectively and i is the index that covers each of the discretized areas. This step inserts limitations to the frequency range of interest. For a certain wavelength to be sufficiently represented, there need to be a minimum of six elements within this wavelength [5]. With this, it is possible to draw a dependency between discretization size and highest frequency where this model is valid.

To thoroughly study the sound field created by the impact, the radiated pressure should be studied for many points around the plate. However, to facilitate the evaluation of the efficiency of the control applied, these many points should be expressed by one value which is able to characterize the properties of the radiating structure. In this work, an evaluation of the total radiated sound power was selected to perform this evaluation. The radiated sound power of a structure is expressed as [5]:

$$W = \int_{S_r} I_r\, dS_r \tag{2.29}$$

where S_r is the receiving surface where the intensity is calculated and I_r is the intensity. In the far field, this intensity can also be written as:

$$I_r = \frac{1}{T} \int_0^T \frac{p_r(t)^2}{\rho_0 c_0} dt \tag{2.30}$$

where $p_r(t)$ is the pressure at a moment in time for a specific receiving position and T is the total integration time. For this thesis, a sphere with radius R was used as the receiving surface of the impact sound. Since this sphere was also solved numerically, it was discretized. This inserts a new limitation on the maximum frequency which can be sufficiently expressed, which is expressed similarly to the error of the plate discretization. The whole equation for the radiated sound power considering the discretizations and with equation 2.28 thus becomes:

$$W = \sum_{r=1}^{N_r} \Delta A_r \sum_{t=1}^{T} \frac{\rho_0}{c_0} \frac{\Delta t}{4\pi^2} \left(\sum_{i=1}^{S/dxdy} \frac{\ddot{\xi}(t, r_{s,i})\, dx\, dy}{|R_r - r_{s,i}|} \right)^2 \tag{2.31}$$

where ΔA_r represents the area that each receiving position occupies of the receiving half-sphere, N_r is the number of receiving positions and R_r is the coordinate of one specific receiving position. Thus, it is possible to notice that to calculate the total sound power from a simply supported plate, one must know the time signature of the acceleration of the top surface of the plate and use many receiving positions around this surface.

2.2 Active Noise Control

The concept of active noise control (ANC), presented in a patent by Paul Lueg in 1936, has as its main basis the control of sound coming from a source by the introduction of one or more secondary source of sound. Although the concept has been further developed and enhanced since, this idea is still fundamental to this method [14, 15] .

The physical process that allows this is interference, and thus, with the introduction of a secondary sound field whose properties are specifically determined, it is possible to control aspects of the resulting sound field, which is given by the interference between the primary and secondary ones. The way this concept will be applied to this work is through the addition of a determined active force to the plate of the studied system, with the intention of controlling the sound radiated from this plate. However, before this can be done, it is necessary to find the optimal time signature of the active force to be used. In order to find this optimal force, the Least Mean Square algorithm was applied and, therefore it will be described next.

2.2.1 The Least Mean Square algorithm

The LMS algorithm is a tool used in filter design that relies on an iterative process to find the optimal filter coefficients that minimize a predetermined error function [16], as illustrated in figure 2.4.

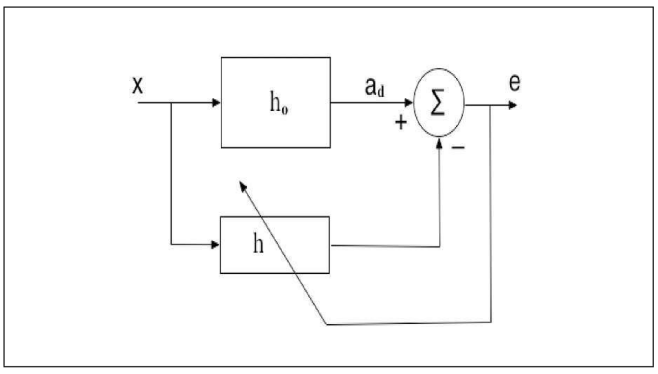

Figure 2.4: Block diagram of an adaptive filter taken from [16].

The fundamental concept behind the LMS algorithm is to update the filter coefficients by amounts proportional to the steepest gradient of the mean square error presented, hence the algorithm's name, at the current time step [16]. The error used in the algorithm is the difference between the output of the system, also called desired signal, and the output of the designed finite impulse response (FIR) filter, which is expressed as:

$$e(n) = a_d(n) - \sum_{i=1}^{I} x(n-i)h(i) \tag{2.32}$$

where e is the error at the time step n, a_d is the desired signal at this time step, x is the input signal observed, h is the filter coefficients and I is the length of the filter, which is the length of the FIR filter. The sum in equation 2.32 is the convolution between the input signal until the current time step and the designed filter, which in vector form is represented as:

$$e(n) = a_d(n) - \mathbf{h}^T(n)\,\mathbf{x}(n) \tag{2.33}$$

where T indicated the transpose of the vector, which are

$$\mathbf{h}^T(n) = \Big[h_1(n), h_2(n), ..., h_I(n)\Big] \tag{2.34}$$

and

$$\mathbf{x}^T(n) = \Big[x(n), x(n-1), ..., x(n-I)\Big] \tag{2.35}$$

With the error function defined, it is thus necessary to find the filter coefficients that minimize this function. As mentioned before, the LMS algorithm uses the mean square error as a criterion for this. Thus the cost function for this algorithm is expressed as:

$$C(n) = E\Big[e^2(n)\Big] = E\Big[\Big(a_d(n) - \mathbf{h}^T(n)\,\mathbf{x}(n)\Big)^2\Big] \tag{2.36}$$

where C is the cost function, $E\Big[e^2(n)\Big]$ is the expected value of the error. This leads to the analysis that the cost function is a quadratic equation in terms of result from the convolution of the filter coefficients and the input signal. Hence, the concept of the steepest decline of the filter coefficients can be followed to reach the global minimum of the function. One can express the concept of steepest decline through the gradient of the cost function:

$$\nabla \cdot C(n) = \frac{\partial E\Big[e^2(n)\Big]}{\partial h_i} = 2E\left[e(n)\frac{\partial e(n)}{\partial h_i}\right] = -2E[e(n)x(n-i)] \tag{2.37}$$

This gradient allows for the formulation of the iterative method to find the optimal filter coefficients, which is written as:

$$\mathbf{h}(n+1) = \mathbf{h}(n) - \alpha\nabla C(n) = \mathbf{h}(n) - 2\alpha E[e(n)x(n-i)] \tag{2.38}$$

where α is a weighting factor that determines the step size of the process. The expected value of the error often must be estimated. This estimation can be done using the instantaneous value of the gradient for the current time step [16]. This will, on average, adjust the filter coefficients in a way to minimize the mean square error. Equation 2.38 thus becomes:

$$\mathbf{h}(n+1) = \mathbf{h}(n) - \alpha e(n)\mathbf{x}(n) \tag{2.39}$$

With the method defined, it is necessary to find the appropriate step size for the process. This step size influences both the time the algorithm needs to reach the optimal solution as well as the convergence of the algorithm. This influence is that

the smaller the step is, the better the convergence and the longer the time necessary for the solution to be reached. To guarantee convergence, the value of α must be fulfill the following expression:

$$0 < \alpha < \frac{1}{IE[x^2(n)]} \tag{2.40}$$

This algorithm presents a rather low sensitivity to noise due to the use of the average gradient. Hence, if the noise is affecting the instantaneous time step, the average will still lead towards the global minimum, only requiring a longer time to reach it.

When applying the LMS algorithm to this work, it can be sketched as illustrated in figure 2.5

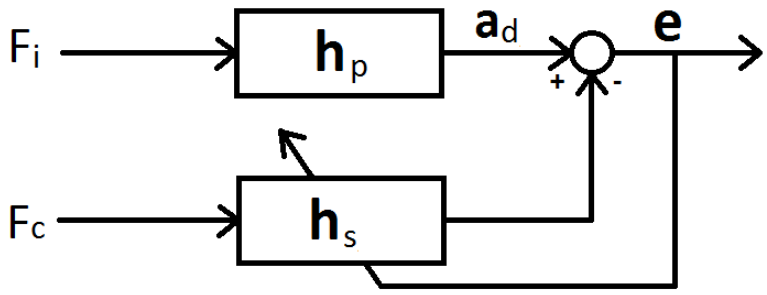

Figure 2.5: Sketch of how the LMS algorithm is applied in this work.

where F_i is the impact and viscous forces summed together, F_c is the active force to be used, h_p is the primary impulse response which means the impulse response related to the point of contact between sphere and plate, and h_s is the secondary impulse response which means the impulse response related to the point where the active force is applied. Both these impulse responses are calculated as shown in section 2.1.3

2.2.2 Force identification method based on LMS algorithm

The main application of the LMS algorithm in this work is to identify the optimal control force to be applied on a specific position of the plate. This means that the filter coefficients can be found by means of the theoretical formulations presented in equation 2.25b, and thus, the input to the system is the desired result. Upon evaluation of the derivation of the LMS algorithm, one notices the need to change only the step where the gradient is calculated in order to obtain the expression that will find the optimal input instead of filter coefficients [16]. Expression 2.37 thus becomes:

$$\nabla \cdot C(n) = \frac{\partial E\left[e^2(n)\right]}{\partial x_i} = 2E\left[e(n)\frac{\partial e(n)}{\partial x_i}\right] = -2E[e(n)h(i)] \tag{2.41}$$

Leading to the following formulation of the iterative process:

$$\mathbf{x}(n+1) = \mathbf{x}(n) - 2\alpha E[e(n)h(i)] \tag{2.42}$$

Now however, a problem with the expected value arises. Previously, the quadratic error would reach the desired level of reduction if the input signal was sufficiently long to obtain a good enough average of the expected value. In the new situation presented in this section, the input is cut off and each unknown input value, $x(n)$ will only be updated I times due to the length used for the FIR filter. This limited amount of updates might not be sufficient to reach the desired optimum point. A trick, presented in [16],that can be applied to solve this problem is to use only a part of the input signal, with the length N, and periodically repeat the filter coefficients with a period length of N as well as the desired signal. This will create an analogy to the standard LMS algorithm, permitting the analogical description of the iterative process as:

$$\mathbf{x}(n+1) = \mathbf{x}(n) - \alpha e(n)\mathbf{h}(n) \tag{2.43}$$

The length used for the input value must be, in practice, at least twice that of the filter length I. This is because the first I values of the desired signal are also influenced by values outside of the observation window (which has the length of N).

2.2.3 Multidegree of freedom LMS

Since the LMS algorithm will be applied to find the optimal force to reduce the radiated sound of the plate, the system should not be analyzed only for one receiving position but for many points around the plate that can sufficiently recreate the sound power from the plate. For each receiving position, there is a specific impulse response which represents one input to the LMS algorithm. The LMS algorithm presented previously is limited to one input and thus needs to be generalized in order to function for multiple inputs [17]. To do this, it is first necessary to specify the error for each receiving position:

$$e_r(n) = a_{dr}(n) - \sum_{s=1}^{S} \mathbf{h}_{rs}^T(n)\, \mathbf{x}_s(n) \tag{2.44}$$

The subscript r indicates a specific receiving position, the subscript s indicates an excitation force, therefore $\mathbf{h}_{rs}(n)$ represents the impulse response for a specific excitation force and receiving position at the current time step, and S is the total amount of excitation forces. The error in equation 2.44 is then used to update the force coefficients. However, given that there are multiple forces, an average of the gradient is performed to find the average optimal direction towards the minimum. The process is then formulated as:

$$\mathbf{x}_s(n+1) = \mathbf{x}_s(n) - \langle \alpha_r e_r(n)\mathbf{h}_{rs}(n) \rangle \tag{2.45}$$

The $\langle\rangle$ symbol represents the average over the receiving positions. It is important to emphasize that the current time step n must be larger than the FIR filter length. One last consideration is the limit of the weighting factor α, which due to the increase

in degrees of freedom, must be defined with more restriction. The following relation expresses this:

$$0 < \alpha < \left(\frac{N}{R} \sum_{r=1}^{R} \sum_{i=0}^{I} |\mathbf{h}_{rs}(i)|^2 \right)^{-1} \tag{2.46}$$

where N is the length of the input signal and R is the number of receiving positions. These alterations were applied to the LMS algorithm used in this work and the final sketch of the used algorithm is shown in figure 2.6

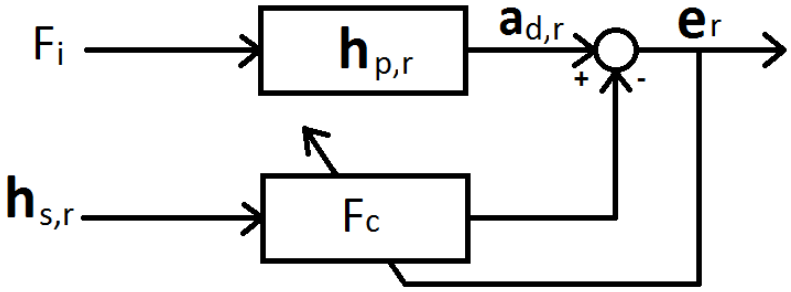

Figure 2.6: Sketch of the LMS algorithm used in this work after the necessary alterations

3

Simulation setup and results

In this chapter, the setup used to reach the goal of this work as well as the reasoning behind certain decisions are discussed. Consideration to the limitations presented in the theory and applicability of the equations presented in that chapter are reviewed. The necessary calculations to find the inputs to the main algorithm used in this work are also shown. Results obtained from the simulations are presented in the pertinent subsections.

3.1 Definition of plate and sphere to be studied

The simply supported plate selected for the simulations performed in this study is made of Plexiglas, with a length of 0.8 m, a width of 0.7 m and a thickness of 0.035 m. The sphere chosen is a made of steel with a radius of 0.02 m. These are illustrated in figures 3.1 and 3.2 and the detailed material properties used in the calculations are presented in table 3.1.

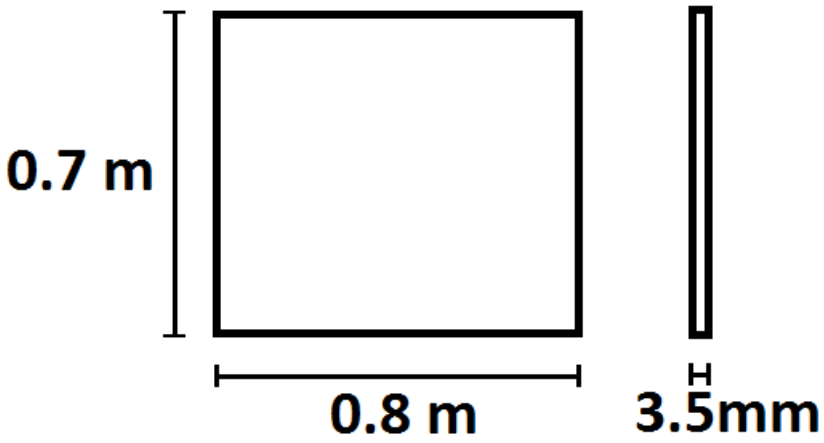

Figure 3.1: Schematic depiction of the studied plate with dimensions.

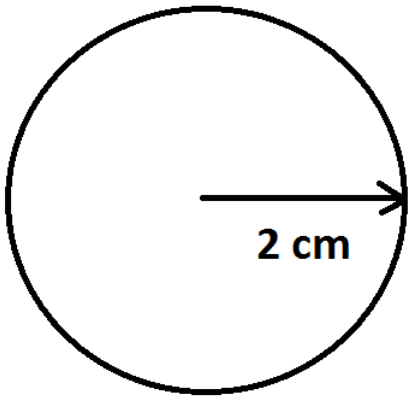

Figure 3.2: Schematic depiction of the studied sphere with dimensions.

Table 3.1: Overview of material properties

Material	Plexiglas	Steel
Density (kg/m^3)	1150	7800
Elastic modulus (N/m^2)	$5.6 \cdot 10^9$	$210 \cdot 10^9$
Poisson's ratio	0.37	0.31
Loss factor	0.02	-
Viscous damping	12	-

The main reason for the choices presented above were simplicity and availability of the evaluated specimens. Both steel and Plexiglas are largely available and used in today's industry.

3.2 Initial conditions and defined calculation parameters

As the initial conditions for the studied case, the sphere was dropped at a height of 5 cm from the plate surface, with no initial velocity. The plate is initially at rest and has it's top surface at the xy-plane of the used coordinate system. The point of impact between sphere and plate was varied, along with the point where the control force is applied, in order to study control effort and effectiveness of the proposed control method. The receiving half-sphere selected for this work has a 10 m radius. This is to guarantee that assumptions relying on far-field pressure are satisfied.

Lastly, a value of $\alpha = -\frac{1}{3}$ was used for the HHT algorithm. In all simulations, the gravitational constant of $g = 9.81$ m/s^2, the speed of sound $c_0 = 340$ m/s and the air density $\rho_0 = 1.2$ kg/m^3 were used. Lastly, a time step of size $\Delta t = 1 \cdot 10^{-6} s$ was defined in order to properly represent an impact, given its short duration. This time step used only for the estimation of the impact force which will be shown next, for

the LMS-algorithm, the time step $\Delta t = 2 \cdot 10^{-4} s$ was chosen to reduce the computational effort of the simulations.

The determination of the time step size implies the definition of the frequency limit. This frequency limit indicates the maximum eigenfrequency that can be represented with the used time step, implying in a limit to the number of modes used in the modal summation present in the impulse response calculations, shown in section 2.1.3. The limit to the eigenfrequencies is expressed by $\omega_{n,m,max} = \pi/\Delta t$ [3].

3.3 Determination of the input forces

As shown in chapter 2, the impact and viscous forces applied on the plate will vary not only due to the properties and dimensions of the plate and sphere, but also due to the position in which the impact occurs in the plate. This is because of the presence of the impulse response in the numerical methods used to find these forces, since these responses are dependent of the position in which the impact occurs.

Therefore, a analysis of the influence of the position was carried out. For this analysis, three positions were selected within the plate. These positions are described in table 3.2 and illustrated in figure 3.3.

With these positions defined, the numerical methods described in section 2.1.2 were applied. For each time step, the condition of relative distance between plate and sphere being smaller than zero was verified. This was performed to guarantee that the contact was still occurring. Next, the equation describing the sphere's motion was solved using the Newton-Rhapson method with this relative displacement as the variable that the method solved for. This method was repeated until the error between successive iterations was smaller than a determined tolerance. This tolerance was defined to be equal to the time step used in the process. Once this method reached its goal, the values for the relative displacement, velocity and acceleration were updated using the Hilber-Hughes-Taylor method. Figure 3.4 shows the obtained impact forces for the three aforementioned positions and figure 3.5 shows the obtained viscous forces for the same positions.

Table 3.2: Impact position coordinates

Position	Coordinates
Impact Position 1	(0,4; 0,35)
Impact Position 2	(0,6; 0,6)
Impact Position 3	(0,3; 0,15)

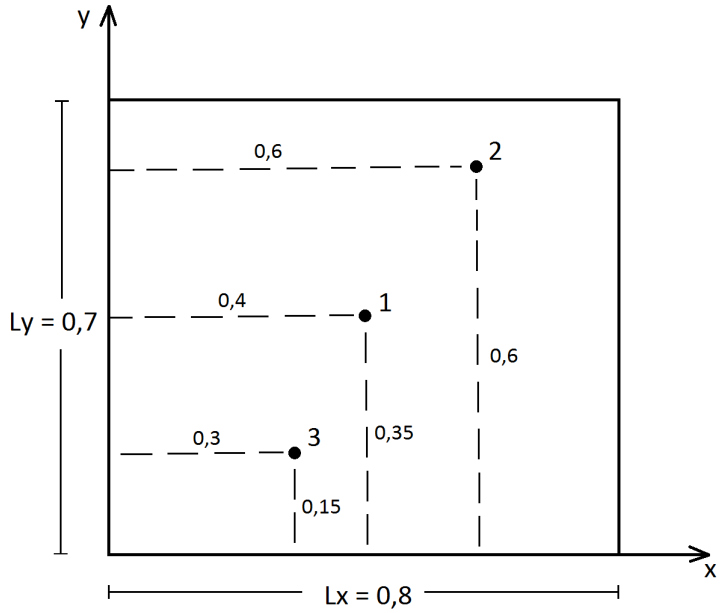

Figure 3.3: Sketch of the simply supported plate and the different impact positions that were simulated

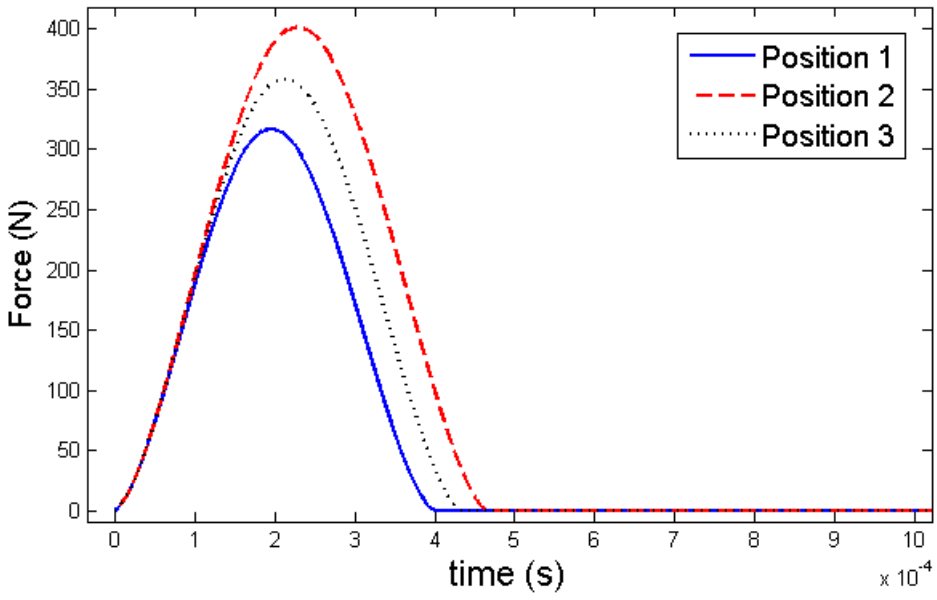

Figure 3.4: Impact forces for different impact positions

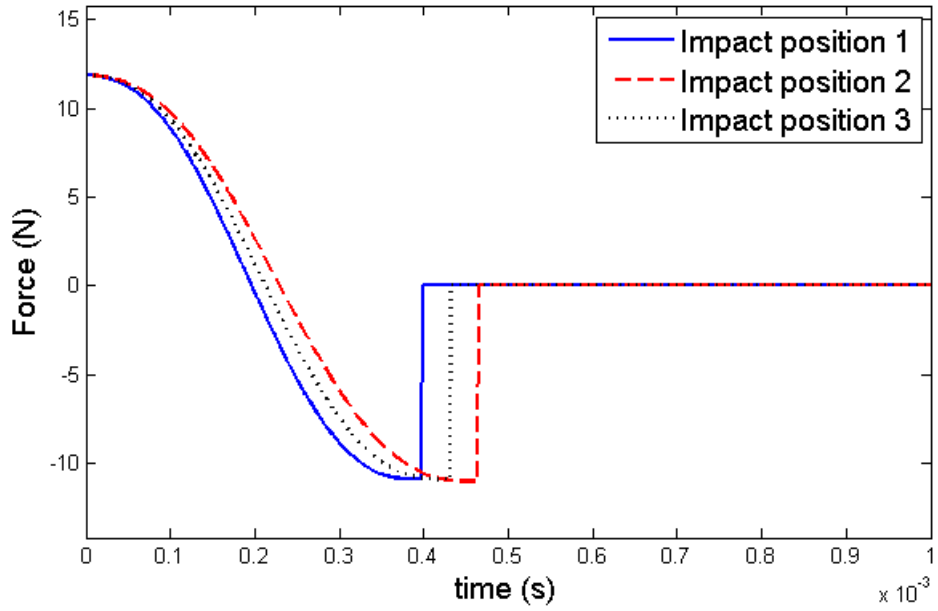

Figure 3.5: Viscous forces for different impact positions

Evaluating figure 3.3 and 3.4 it is possible to notice a specific pattern in the behavior of the impact forces in relation to the position of the impact within the plate. This pattern is that the closer the impact occurs to the borders, the larger the magnitude of the impact force. This is expected once the positions closer to the borders present a higher stiffness and therefore will create larger relative displacements between sphere and plate. Another expected result seen in the impact forces is that the larger the magnitude of the force, the longer the impact time is. This is expected because it takes longer for the deformations related to the force to return to the initial state.

From figure 3.5 it is possible to notice that the different positions do not affect the magnitude of the force. However, there is an influence related to the impact time. This is related to the fact that this force is dependent of the relative velocity, indicating that shorter impact times have quicker changes in this relative velocity, as expected.

It was also considered important to verify the frequency content of the input to the system evaluated. Therefore, a Fourier transform of the sum of the impact and viscous forces, which is the total input force, was performed. With the knowledge that only one impact was being simulated, zero padding was used to improve the frequency resolution of the frequency domain representations of the total input forces. Figure 3.6 shows the obtained total input force in the frequency domain.

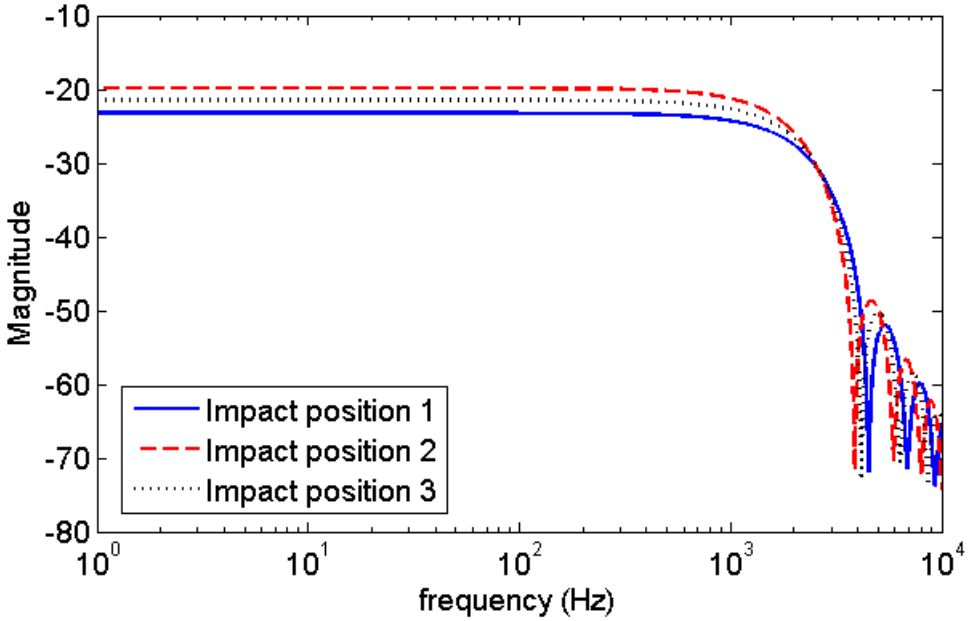

Figure 3.6: Frequency domain representation of total input force

3.4 Frequency study

A characteristic of an impulsive force is that their behavior in the frequency domain mimics that of a low-pass filter. Since the total input force into the system will present the general appearance of an impulsive forces, this is the behavior seen in figure 3.6. The frequency in which the filter begins to attenuate the signal, called the cutoff frequency, for the low-pass filters in figure 3.6 is around 3 kHz. Also, the different values for magnitudes are directly related to the magnitude of the impact forces, as seen in figure 3.4.

Another analysis to study the behavior of the plate itself was performed. This was an evaluation of the plate's radiation efficiency. This parameter is used to evaluate the characteristics of the plate as a radiator by comparing the radiation from the plate to that of a plane radiator. Figure 3.7 shows the radiation efficiency of the plate studied.

From figure 3.7 it is possible to extract the coincidence frequency of the plate, which is the frequency at which the plate becomes a more efficient radiator. For the studied case, this frequency is around 1 kHz. It is also noticeable that the first mode radiates very well, having a radiation efficiency close to 1. Considering the shape of the first mode, this leads to the observation that this plate's radiation will resemble that of a monopole. Thus, the radiation resulting from this plate will be quite omnidirectional.

The time step presented to calculate the total input force was chosen based on the need of a very small step to represent the impact. However, it leads to quite a large

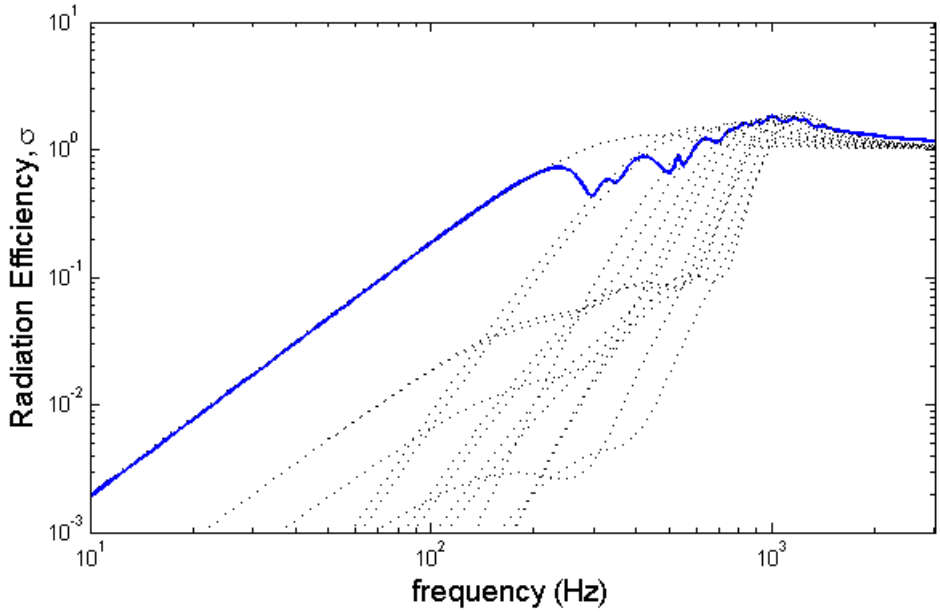

Figure 3.7: Radiation efficiency of the studied plate. The solid blue line represents the efficiency achieved from modal superposition and the dotted black lines are the efficiencies of the first 15 modes separately.

studied frequency range, up to 500 kHz. With the characteristic of both the plate and the excitation that were described above, a new frequency range of interest was determined. This frequency range was determined to be up to 2.5 kHz, leading to a new time step of $\Delta t = 2 \cdot 10^{-4} s$ which is to be used in the LMS algorithm. Thus, the total input force was resampled to match this time step and the calculations of the transfer function was performed using this value as well.

4

LMS Algorithm

Once the magnitude and time behavior of the impact force are determined, this force is used as an input to the LMS algorithm. The transfer functions from the forces acting on the plate to the pressure at a receiving point are then calculated to obtain the desired signal for the LMS to mimic. With this information, the LMS algorithm is subsequently performed. In this chapter, the details of this algorithm are described and the results obtained are fully portrayed along with discussions on these results.

4.1 Decription of the applied LMS algorithm

With the conception of the LMS algorithm presented in section 2.2.3, each variable used in the algorithm will be described in this section. First, the time signature of the variable F_t in figure 2.6 was found through the resampling of the total input force of the system for the new time step $\Delta t = 2 \cdot 10^{-4} s$. Figure 4.1 presents this for one of the impact positions discussed in section 3.3.

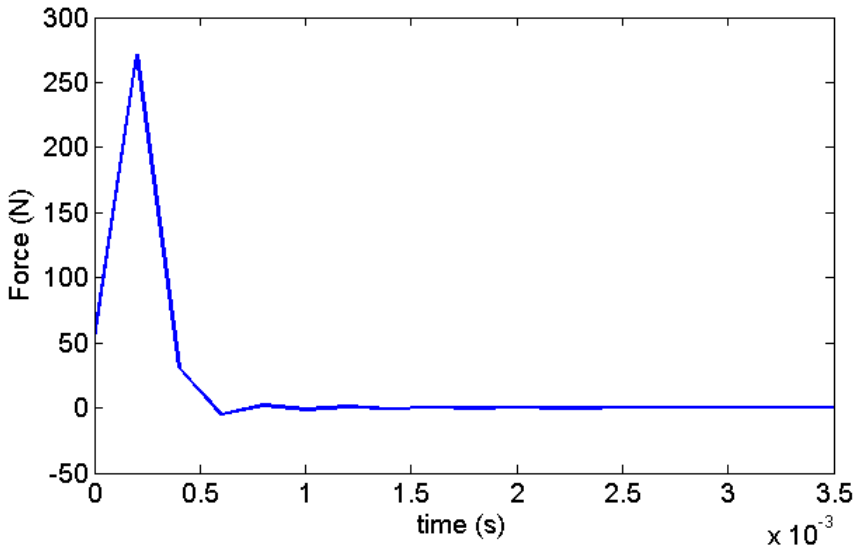

Figure 4.1: Example of the resampled total force used as an input to the LMS algorithm.

Following this, the transfer functions for the total input force and each of the re-

ceiving positions was calculated. In figure 2.6 this is represented by the variable $h_{p,r}$. The time step for these was the same as the one of the resampled input forces and the length chosen for these functions was defined to be 1 second long since this duration was considered to present a large enough attenuation of the response. For the calculations, the frequency limit described in section 3.4 is also applied in the discretization of the plate, used in the Rayleigh integral. A rule of thumb of the finite element method states that at least 6 elements are necessary to properly represent a certain wavelength. Taking the eigenfrequency of highest mode evaluated and the speed of sound for bending waves, the smallest evaluated wavelength is obtained. For the case studied, this lead to a discretization of the plate by a step size of $dx = dy = 7.8125 \cdot 10^{-4}$ m.

The half-sphere used in this work is represented by 513 equidistant discrete points, which means that 513 receiving positions are used in this work to estimate the radiated sound power from the plate. Figure 4.2 presents an example of these transfer functions chosen for a specific receiving point.

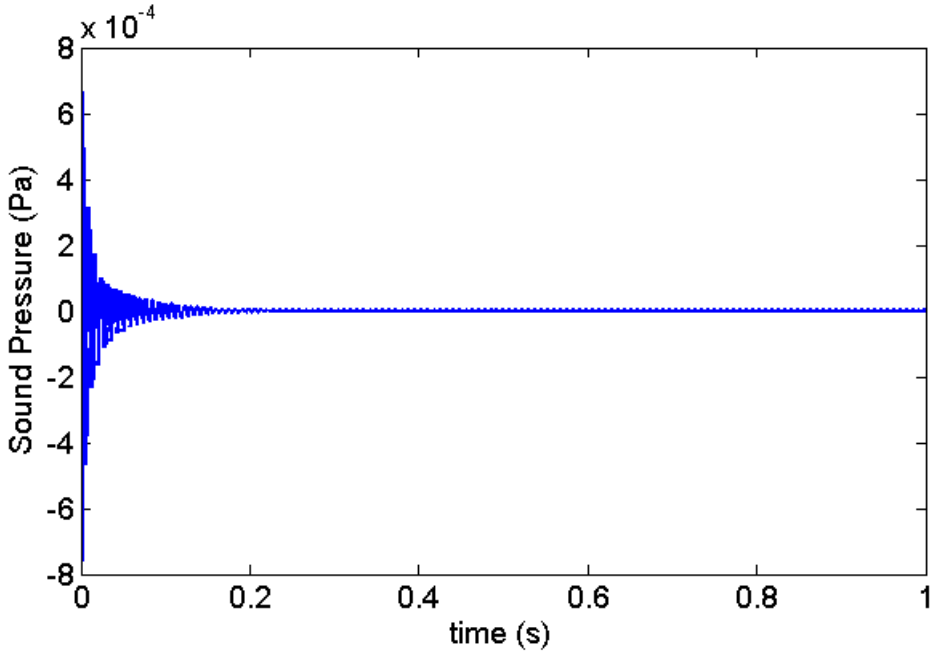

Figure 4.2: Example transfer function for a specific receiving position.

The last step in the calculation of the primary path is the time convolution of both the input force and the transfer function. This was then performed for each of the transfer functions to obtain the desired signals for the LMS to mimic, represented in figure 2.6 this is represented by the variable $a_{d,r}$. This convolution is shown in figure 4.3 for the same receiving position as the one in figure 4.2.

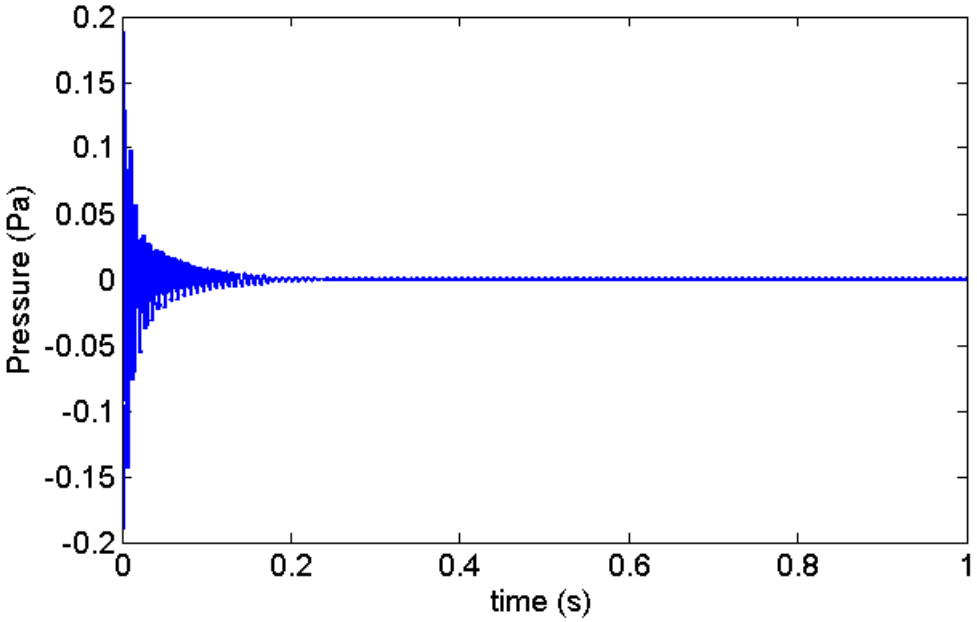

Figure 4.3: Example of the primary path for the same position as shown previously.

This same process used to calculate the transfer function related to the input force, with the same time step and length, was used to calculate the transfer functions between the control positions and the receiving positions. In figure 2.6 this is represented by the variable $h_{s,r}$.

Now with all the variables defined for the LMS, the parameters rulling the overall performance of the algorithm were determined. These parameters were the step size of the algorithm, α, and the number of iterations by which the whole process will be done.

Through trial testing the speed of convergence of the algorithm, the α values were determined. They were found to be in the order of $1 \cdot 10^2$, and thus this value was used in all the simulations performed in this work. As for the amount of iterations, 100 were determined to be sufficient for this work, although different levels of error between iterations were achieved in the simulations. These errors will be presented along with the obtained time signal for the optimal active forces as the results from the simulations.

4.2 Results for impact position 1

In figures 4.4, 4.5, 4.6 and 4.7 the results of the LMS algorithm for impact position 1 and each of the active force positions are presented. The results include the total time signature of the active force, a look at the first 0,1 second in detail and the relative error between each of the iterations of the algorithm.

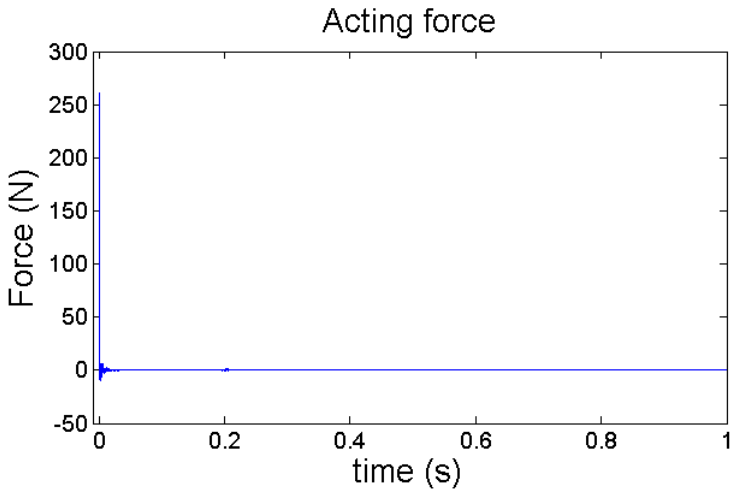

(a) Time signature of the obtained optimal active force

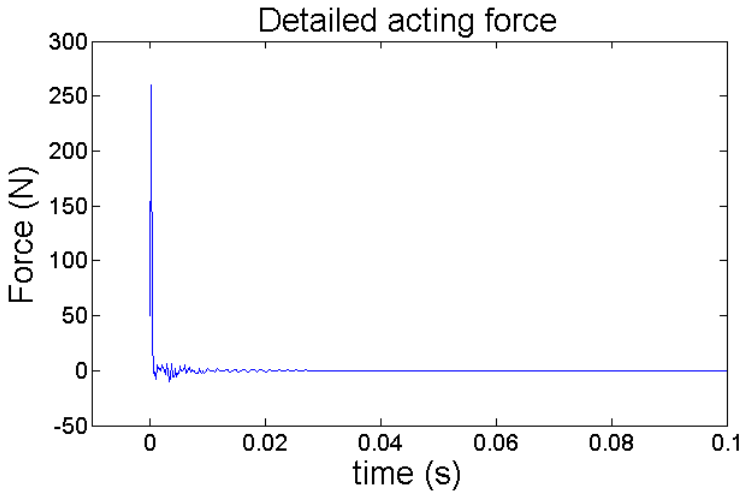

(b) Detailed view of the optimal active force

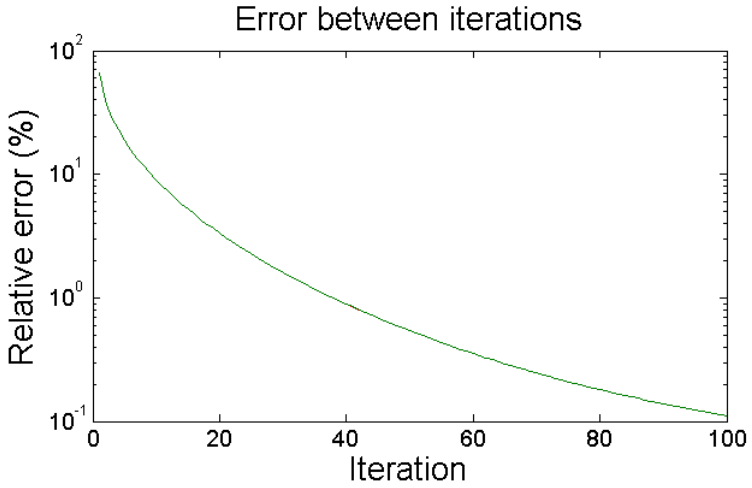

(c) Relative error between each iteration of the LMS algorithm

Figure 4.4: Results obtained from the simulation of an impact applied in position 1 with an active force applied in control position 1.

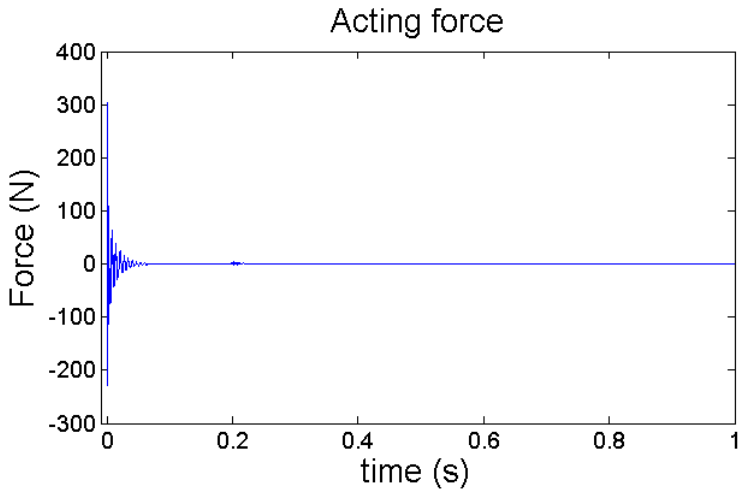

(a) Time signature of the obtained optimal active force

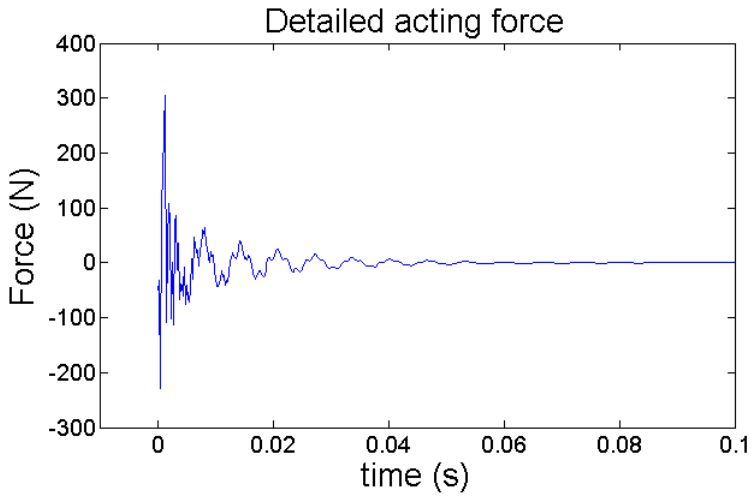

(b) Detailed view of the optimal active force

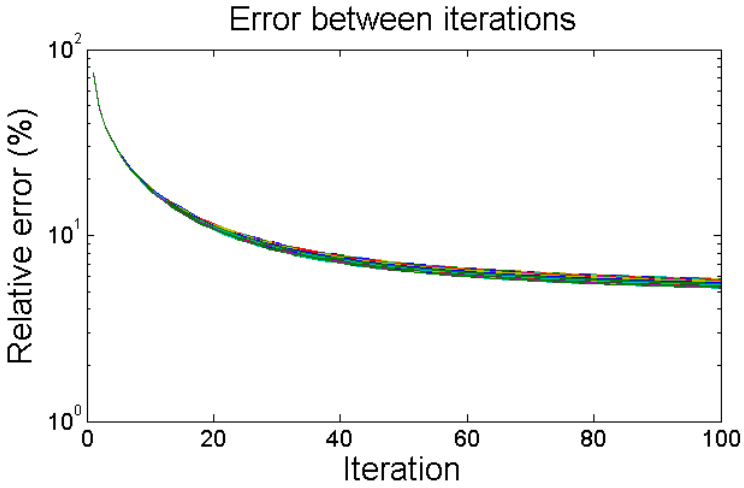

(c) Relative error between each iteration of the LMS algorithm

Figure 4.5: Results obtained from the simulation of an impact applied in position 1 with an active force applied in control position 2.

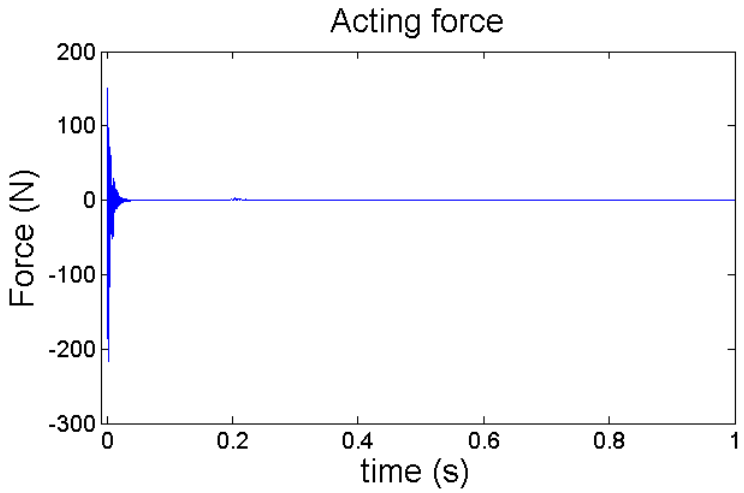

(a) Time signature of the obtained optimal active force

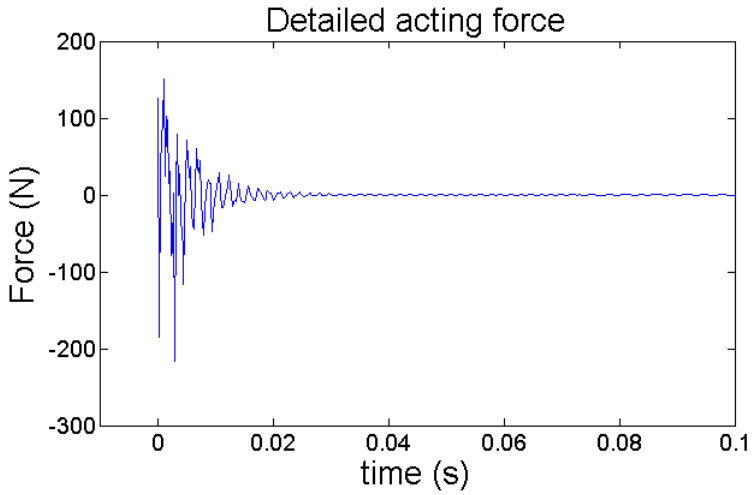

(b) Detailed view of the optimal active force

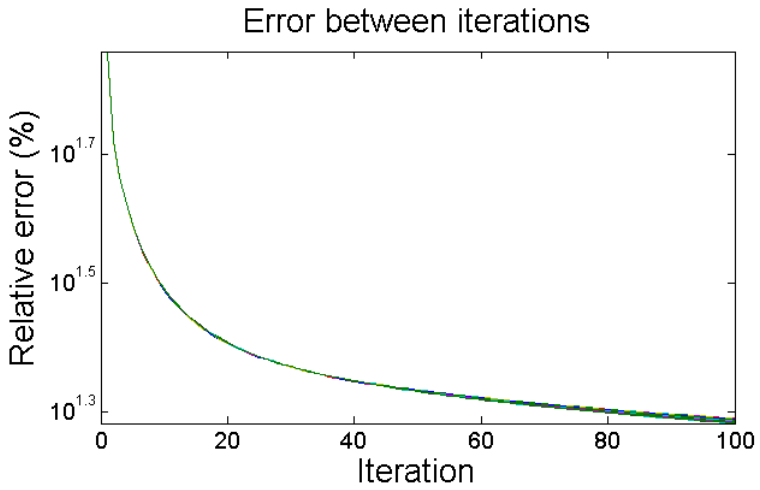

(c) Relative error between each iteration of the LMS algorithm

Figure 4.6: Results obtained from the simulation of an impact applied in position 1 with an active force applied in control position 3.

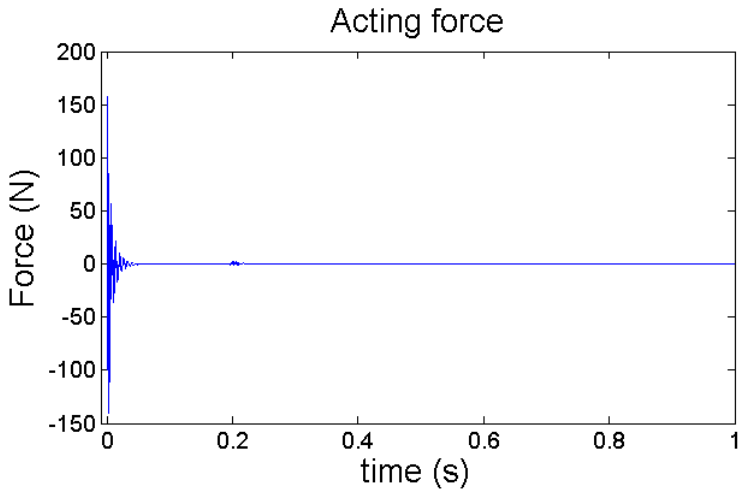

(a) Time signature of the obtained optimal active force

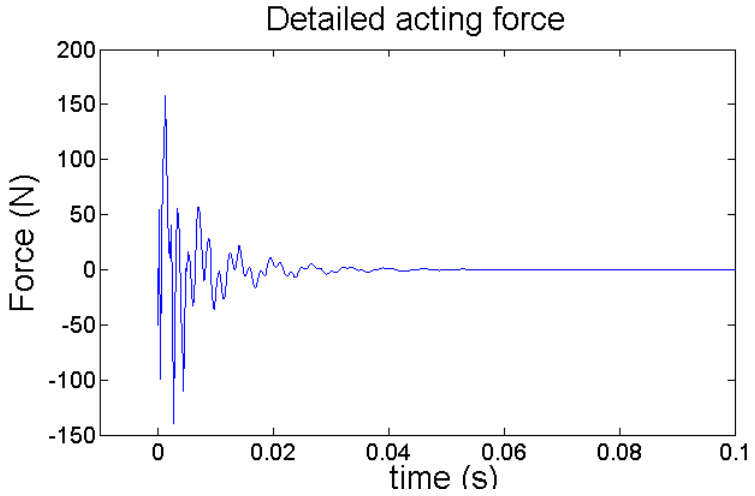

(b) Detailed view of the optimal active force

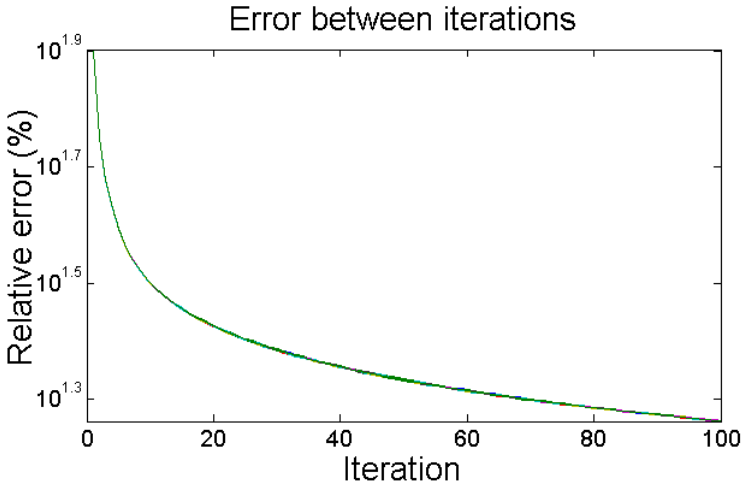

(c) Relative error between each iteration of the LMS algorithm

Figure 4.7: Results obtained from the simulation of an impact applied in position 1 with an active force applied in control position 4.

A lot of information can be extracted from figures 4.4 to 4.7. First, the result when the impact position is the same as the control position, shown in figure 4.4, presents what can be considered the trivial solution. For this case, it is easy to notice that the active force should mimic the input force directly. This would cause a cancellation of the input, and therefore, a very high reduction of the radiated sound power from the plate. The time-signature observed in figure 4.4b shows that the expected result was obtained and thus indicates that the LMS algorithm is working properly. It is worth noting that this active force was recreated from the simulated pressure at the receiving points used in this work.

The active forces obtained when the impact position and control position are not the same have different behaviors than that of the trivial case. All three other cases presented active forces that have a longer time signal. All three also present a decaying behavior, with most of the needed active force lasting only 0,04 seconds. However, they present varying levels of magnitudes, which indicate the control effort. Control position 4 is the one which requires the least effort, followed by control position 3 and, lastly, control position 2 requires the most effort.

Lastly, when evaluating the relative error between iterations for each of the different cases one notices that they all decrease with the more iterations performed. There is also indication that the first case, in figure 4.4, is the one that would benefit more from further iterations. Another aspect seen in figure 4.4c is that this control position holds the lowest relative error presented for impact position 1. The second lowest relative error is presented in 4.5c, which indicates that this control position is the one that obtains the largest reduction in sound power for a non-trivial case. This will be further evaluated in chapter 5.

4.3 Results for impact position 2

In figures 4.8, 4.9, 4.10 and 4.11 the results of the LMS algorithm for impact position 2 and each of the active force positions are presented. The results include the total time signature of the active force, a look at the first 0,1 second in detail and the relative error between each of the iterations of the algorithm.

Impact position 2 presented similar results as impact position 1. First, the trivial case, shown in figure 4.9, behaves as expected, presenting an optimal active force which mimics the input force of the system for this case. As for the other control positions; all present time signals longer than the trivial position, as for the impact in position 1 and they also present the same decaying behavior, lasting up to 0,04 seconds again. As for the magnitudes of these optimal forces, for the cases presented in figures 4.10 and 4.11 a magnitude similar to the ones presented for impact position 1 is found. However, in figure 4.8, it is possible to notice a much lower magnitude than for the other cases studied. This is an interesting result that is also supporting the conclusion that the first mode of the plate is radiating strongly, as discussed in section 3.4, and acting upon it can reduce the sound power very efficiently.

Lastly, as far as the relative errors obtained in this case, a similar trend to that presented in impact case 1 is presented. This is that all cases show a continuous reduction of the relative error and that the trivial case is the one which presents the lowest relative error. One other interesting aspect, seen when comparing figures 4.8c, 4.10c and 4.11c, is the widening of the difference between each error line as the iteration number increases. This means that the relative error becomes more position dependent, since each line represents the error for one specific receiving position. This thus indicates that the active force acts firstly on the first mode of the plate, which is omnidirectional, and then on removing energy from other modes. It is possible to see a larger widening of the difference between positions in the first control position, figure 4.8c, which is probably because this position is suitable for control of very specific modes and is unable to control other modes.

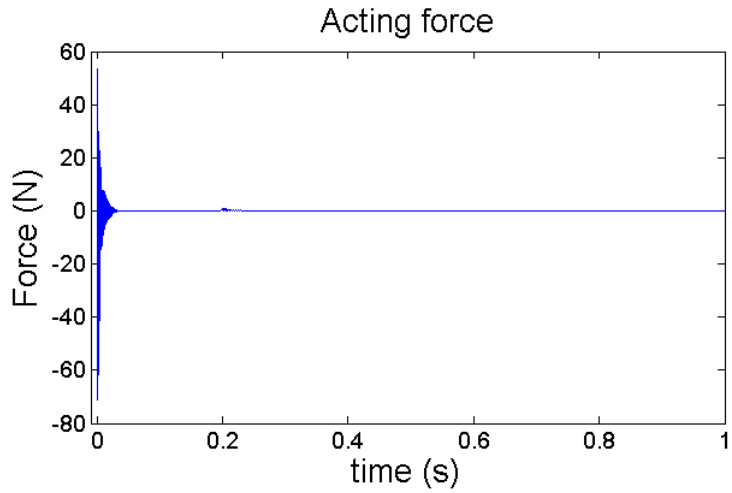

(a) Time signature of the obtained optimal active force

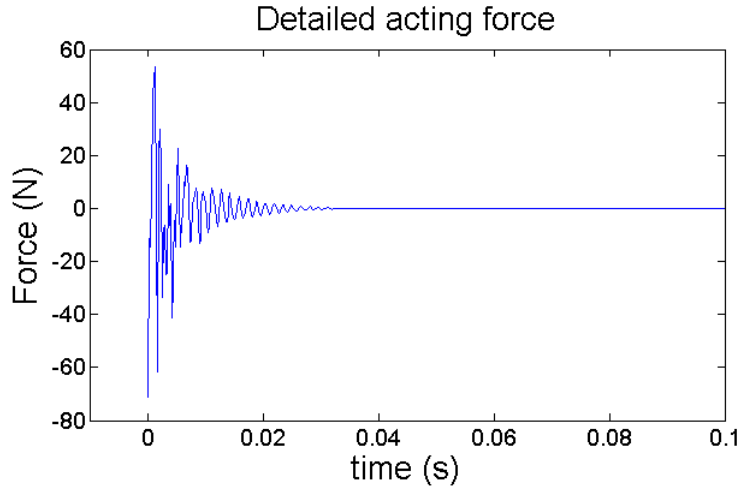

(b) Detailed view of the optimal active force

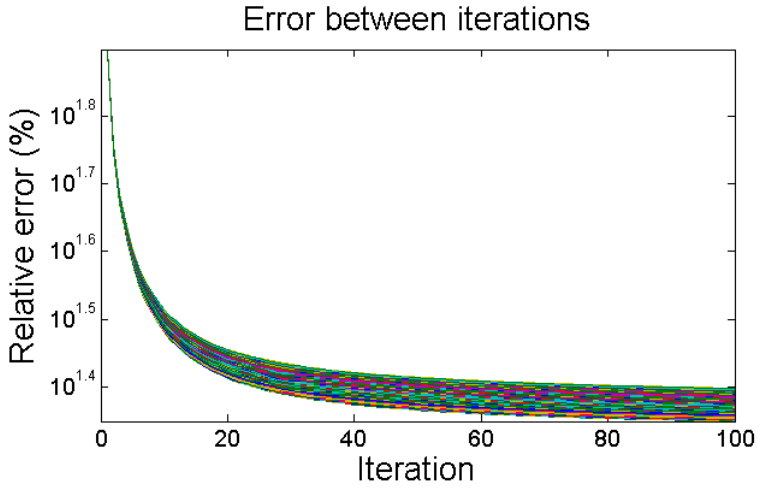

(c) Relative error between each iteration of the LMS algorithm

Figure 4.8: Results obtained from the simulation of an impact applied in position 2 with an active force applied in control position 1.

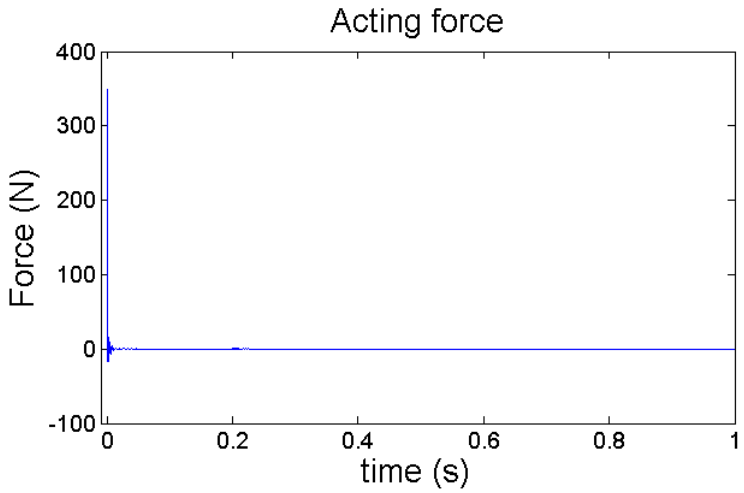

(a) Time signature of the obtained optimal active force

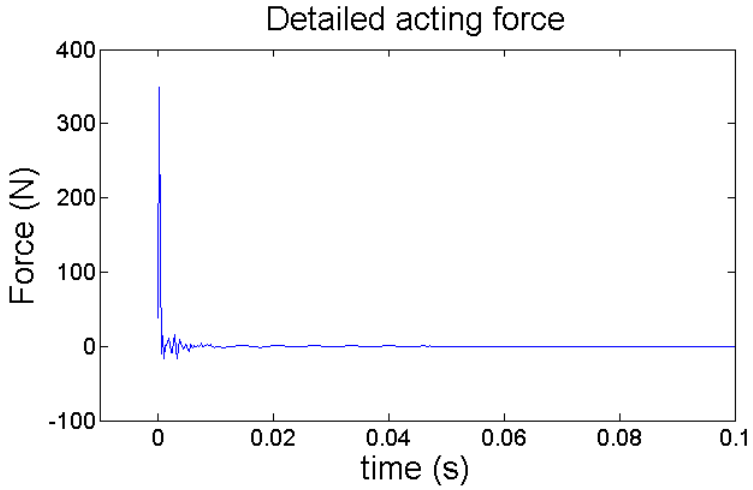

(b) Detailed view of the optimal active force

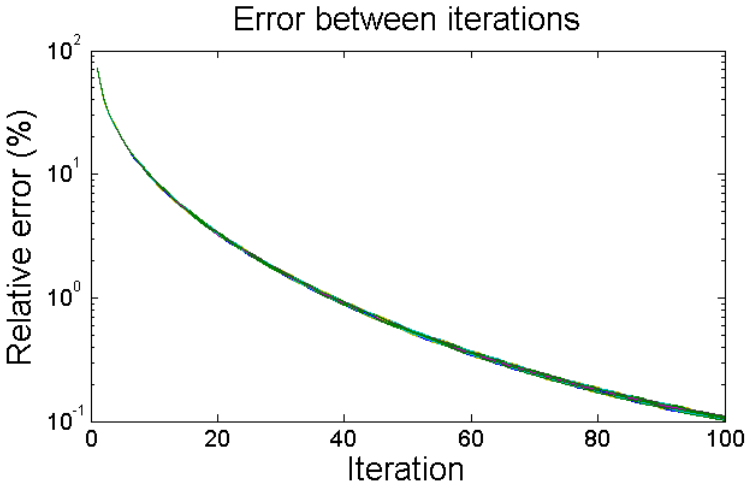

(c) Relative error between each iteration of the LMS algorithm

Figure 4.9: Results obtained from the simulation of an impact applied in position 2 with an active force applied in control position 2.

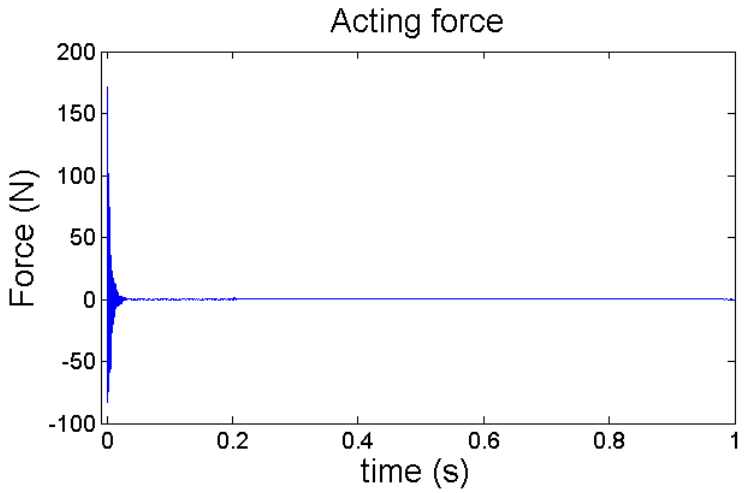

(a) Time signature of the obtained optimal active force

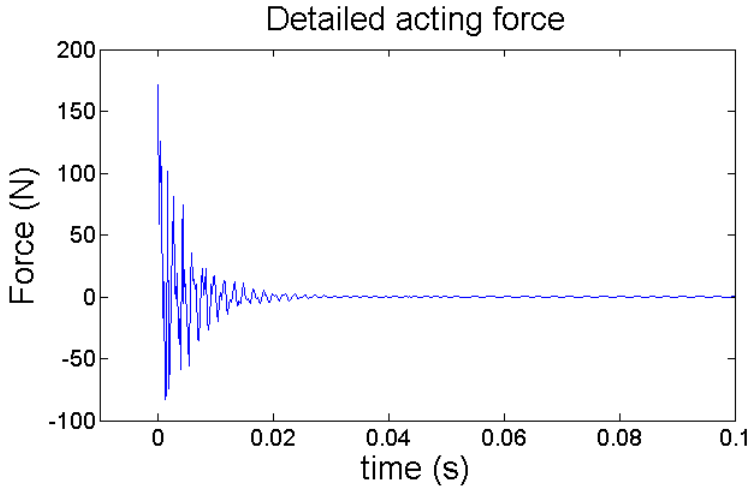

(b) Detailed view of the optimal active force

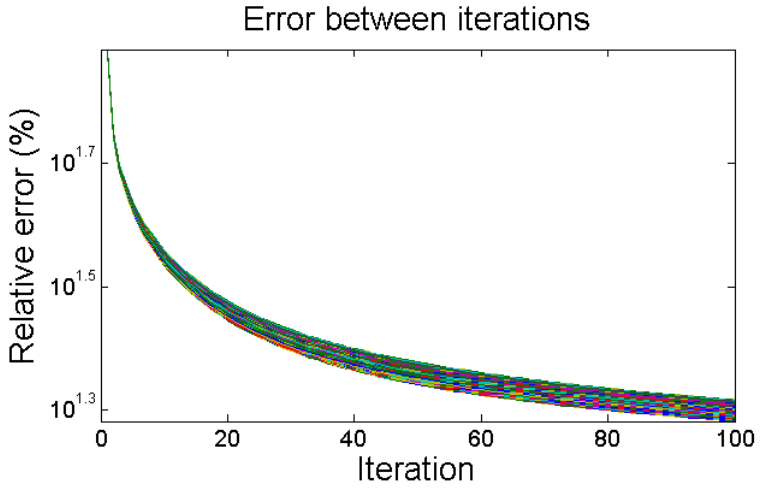

(c) Relative error between each iteration of the LMS algorithm

Figure 4.10: Results obtained from the simulation of an impact applied in position 2 with an active force applied in control position 3.

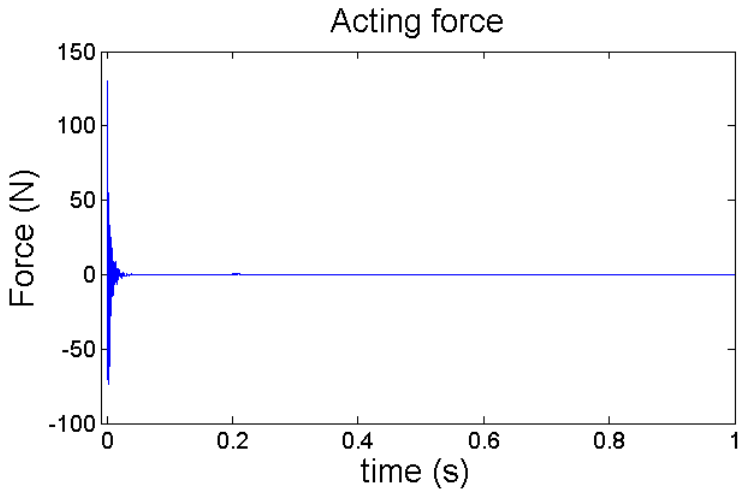

(a) Time signature of the obtained optimal active force

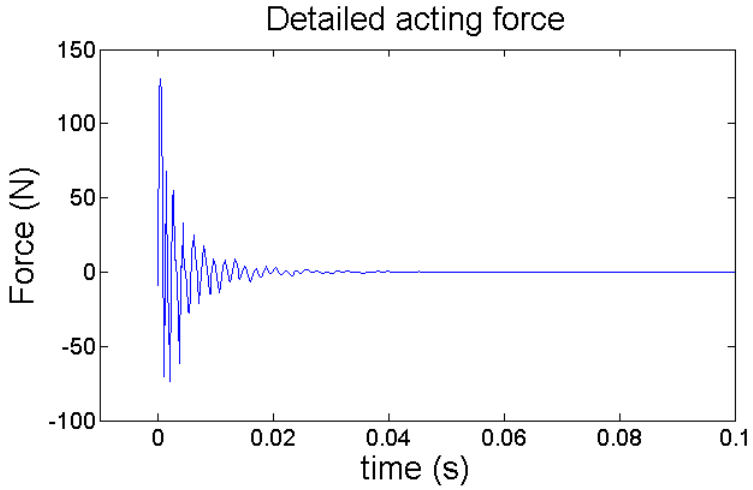

(b) Detailed view of the optimal active force

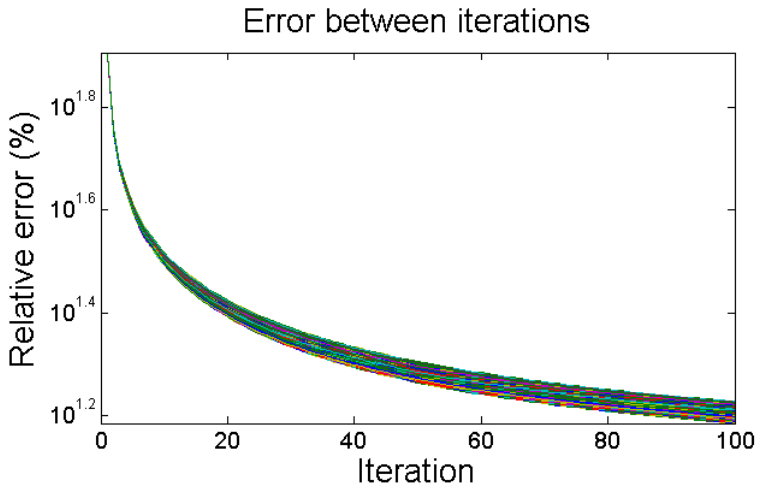

(c) Relative error between each iteration of the LMS algorithm

Figure 4.11: Results obtained from the simulation of an impact applied in position 2 with an active force applied in control position 4.

4.4 Results for impact position 3

In figures 4.12, 4.13, 4.14 and 4.15 the results of the LMS algorithm for impact position 2 and each of the active force positions are presented. The results include the total time signature of the active force, a look at the first 0,1 second in detail and the relative error between each of the iterations of the algorithm.

Again, impact position 3 presented similar results as impact position 1. The trivial case, shown in figure 4.14, behaves as expected once more, presenting an optimal active force which mimics the input force of the system for this case. The other control positions once again display time signals longer than the trivial position, as for the impact in positions 1 and 2. They also have the decaying behavior which was characteristic of the previous impact positions, lasting a maximum of 0,04 seconds. The magnitudes varied as seen previously, with the control position 1, in figure 4.12, being the lowest magnitude needed, as seen for impact position 2.

The relative errors produced in this case have a similar trend to that presented in impact cases 1 and 2. This is that all evaluated positions give a continuous reduction of the relative error and that the trivial case is the one which presents the lowest relative error. The largest difference between these errors is that they all stabilize rather early in the simulation, as shown in figures 4.12c, 4.13c and 4.15c. This indicates that there is no need for such a long simulation and that if smaller values of relative error wish to be achieved, then a different, smaller value of α should be chosen. Lastly, all these relative errors are around the same magnitude. This will be further evaluated and discussed in the following chapter.

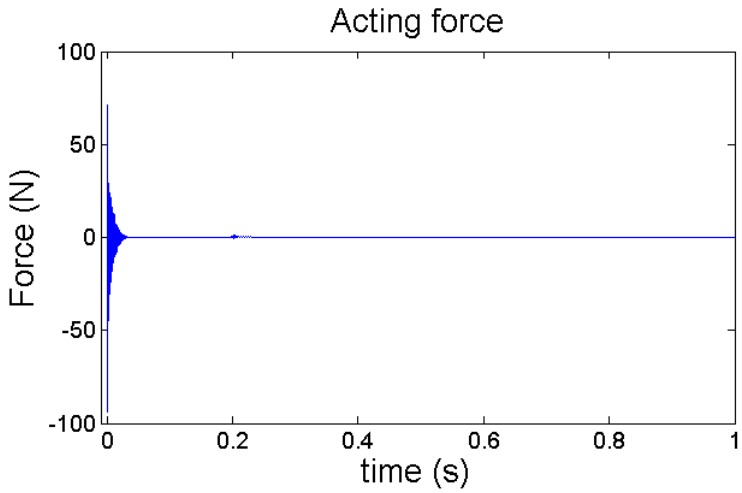

(a) Time signature of the obtained optimal active force

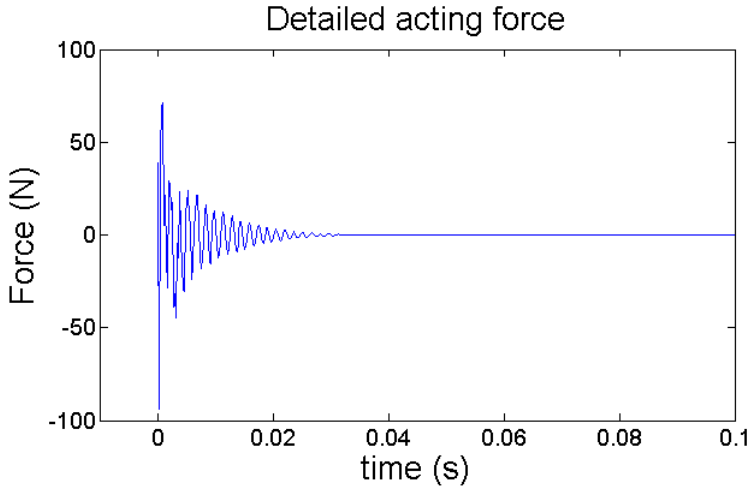

(b) Detailed view of the optimal active force

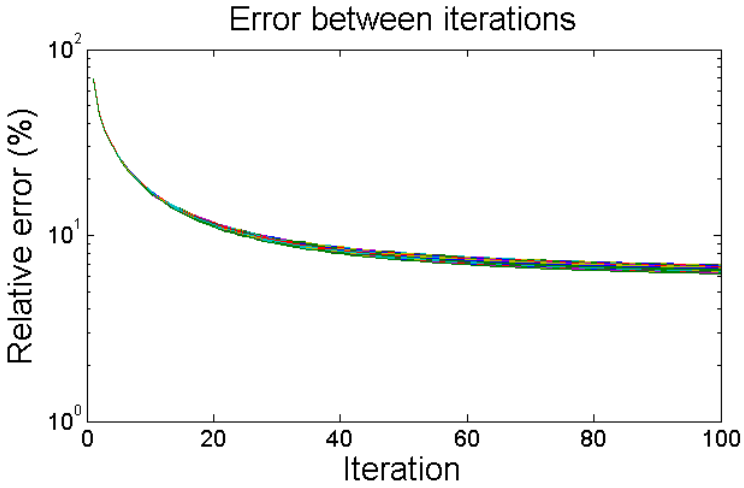

(c) Relative error between each iteration of the LMS algorithm

Figure 4.12: Results obtained from the simulation of an impact applied in position 3 with an active force applied in control position 1.

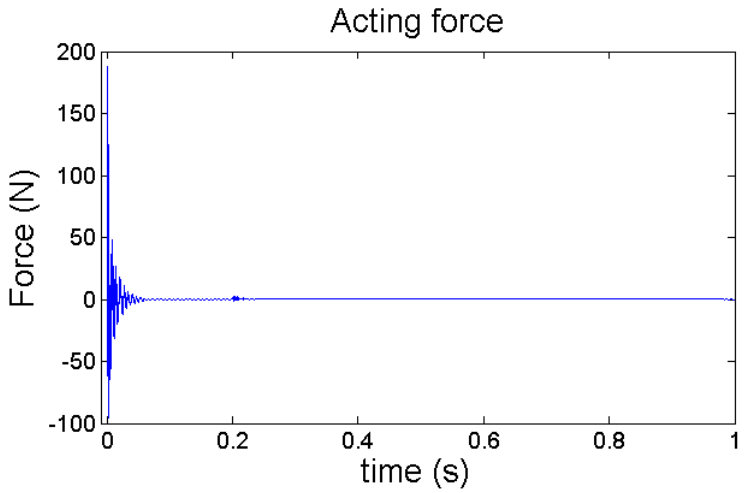

(a) Time signature of the obtained optimal active force

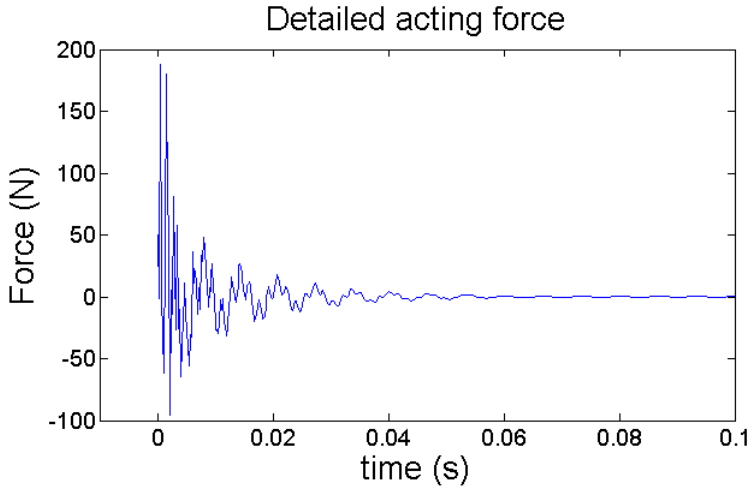

(b) Detailed view of the optimal active force

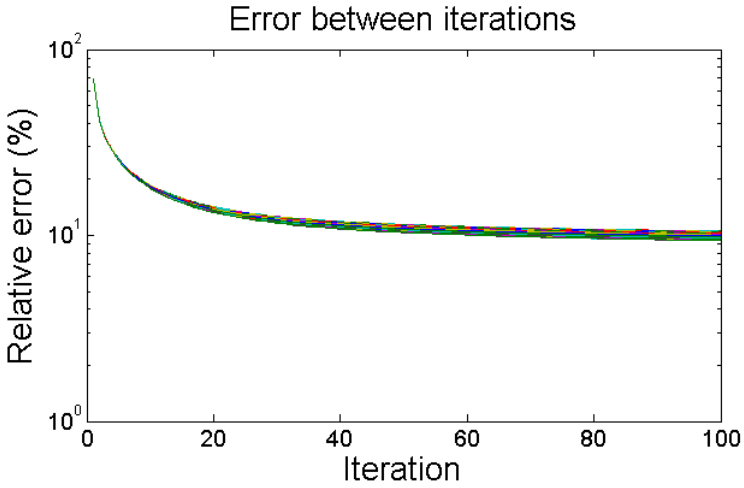

(c) Relative error between each iteration of the LMS algorithm

Figure 4.13: Results obtained from the simulation of an impact applied in position 3 with an active force applied in control position 2.

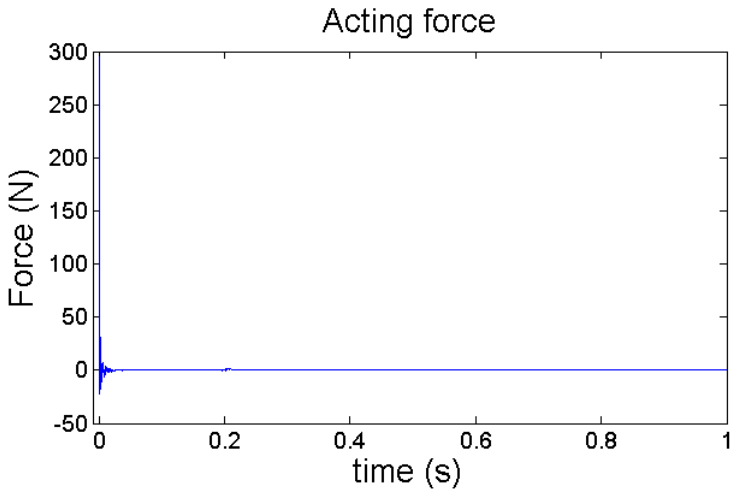

(a) Time signature of the obtained optimal active force

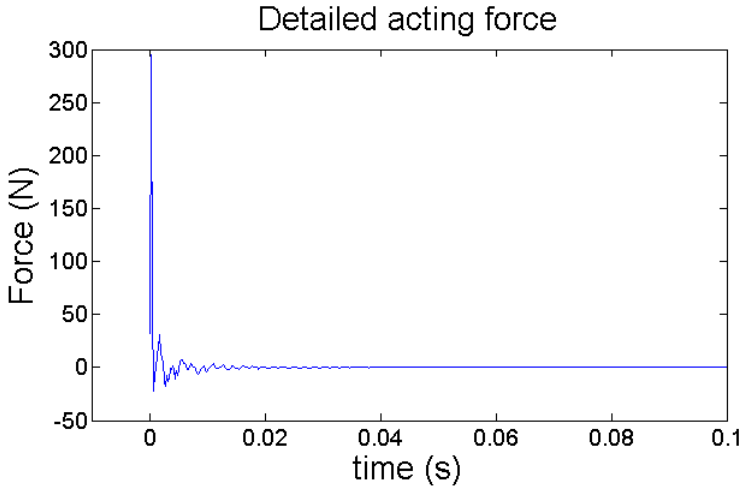

(b) Detailed view of the optimal active force

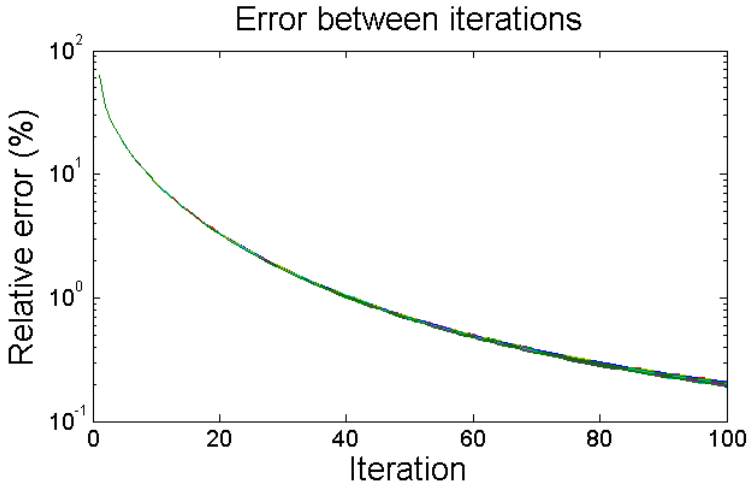

(c) Relative error between each iteration of the LMS algorithm

Figure 4.14: Results obtained from the simulation of an impact applied in position 3 with an active force applied in control position 3.

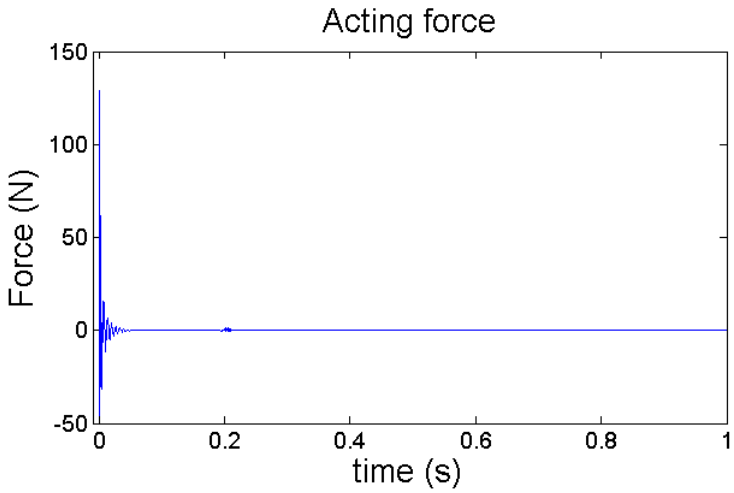

(a) Time signature of the obtained optimal active force

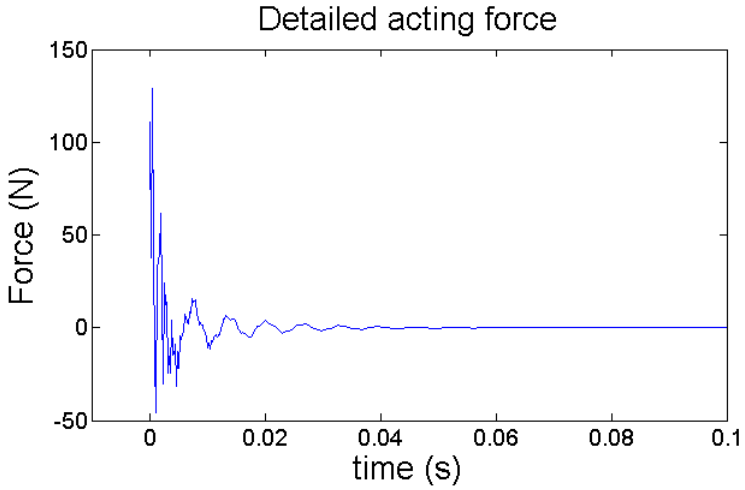

(b) Detailed view of the optimal active force

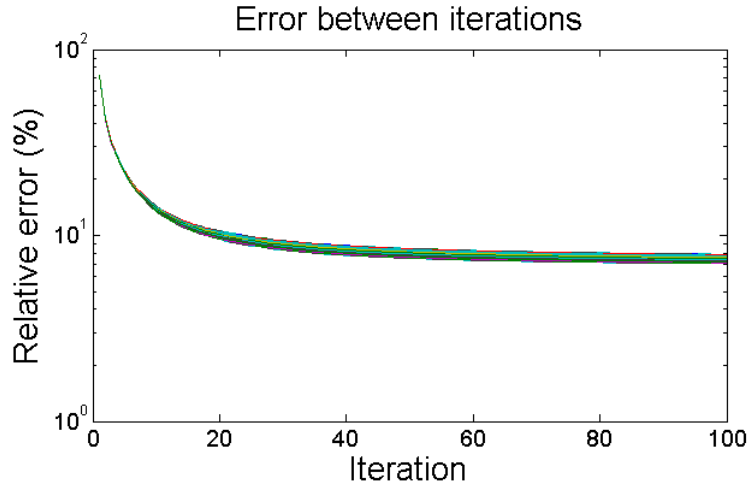

(c) Relative error between each iteration of the LMS algorithm

Figure 4.15: Results obtained from the simulation of an impact applied in position 3 with an active force applied in control position 4.

5

Radiated sound power evaluation

With the obtained active forces presented in chapter 4, it was possible to evaluate the difference between radiated sound power with and without the application of the active force. This radiated sound power was obtained through the summation of the pressure at the receiving points with consideration of the areas that they represent in the half-sphere used in this work. This summation was then performed for situations with and without the presence of the active force and the reduction obtained in the radiated sound power was evaluated in dB. The results for the obtained reduction for all the cases presented in chapter 4 are presented in table 5.1

Table 5.1: Reduction in radiated sound power. The trivial solution reductions are in italic and the largest reductions found for a non-trivial impact position are in bold.

	Control Position 1	Control Position 2	Control Position 3	Control Position 4
Impact Position 1	*-31,1 dB*	**-12,9 dB**	-7,3 dB	-7,6 dB
Impact Position 2	-6,4 dB	*-30,3 dB*	-7,2 dB	**-8,1 dB**
Impact Position 3	**-12 dB**	-10,3 dB	*-27,9 dB*	-11,5 dB

From table 5.1 it is possible to extract and confirm many of the observations made in chapter 4. First, the largest reduction observed for any impact is when the active force is applied in the exact same position as where the impact occurs. This is to be expected, as that is the position where the transfer functions for both the input and the active forces are exactly the same, and thus, allows for the achievement of very high cancellation between the two, subsequently reducing the radiated sound power. Reductions for these cases where around 30 dB, which is quite notable. For cases where the impact and control positions are not the same, reductions were always obtained, varying from 6 to 13 dB. This result also corroborates with what was obtained from the relative errors presented in the previous chapter.

Another observable result from table 5.1 is that no chosen control position was optimal for all impact positions. This also leads to the question of why one positions is better than the other for some cases and not for others. To analyze this matter, a look at the distance between each position was taken. Looking at the first impact position, the control position that obtained the largest amount was the second one. This is the farthest position from the impact point. Also, this is the position that presents the highest magnitude of the optimal active force. For the second impact

position, the largest obtained reduction is from control position 4. This case shows that the closest control point obtained the better results and it is not the one with the highest magnitude of the optimal active force. Lastly, for impact position 3, the control position 1 was the one which obtained the largest reduction. Again this is the closest control position to the impact position, but now it is the active force with the lowest magnitude for this impact position.

The expected result for the best control position depending on impact position is that the closest control position would perform better than the others. This is not what was observed for every case. One possible reason for the discrepancy shown in impact position 1 is that the control position 2 better distributes the energy within the modes of the plate, leading to a more effective reduction in the radiated sound power. Another important point to discuss is that these results could be further improved with the selection of more appropriate α values for the LMS algorithm or through a larger amount of iterations. However, the levels of reduction obtained in the simulations presented in chapter 4 were already considered sufficient as this was to be an initial study on the possibility of using active forces to reduce impact noise.

Furthermore, it is important to make a note on a limitation to possible implementations of the concept developed in this work. To obtain the reductions mentioned here, an actuator with a fast and precise response is necessary. The time step used is very small and the required actuation force can sometimes present a strong oscillatory behavior. This puts a lot of requirements on the actuator that will be used and might even rule out some of the cases evaluated in this work. A more comprehensive study on possible actuators is necessary to fully understand the applicability of these forces, however this was not performed in this thesis.

6
Conclusion

This work demonstrated the applicability of the use of external active forces to control the total sound power from an impact. The studied case chosen was that of an impact between a simply supported plate and a sphere, with the active force applied on the plate. A modification of the LMS algorithm was used to determine the time signature of the force to be applied to the plate. Several different impact and control positions were studied to analyze the behavior of the proposed methodology to these variations.

For all cases evaluated in this work, a reduction of the total radiated sound power was obtained. For cases where the active force was applied in the same position as were the impact occurred, reductions of around 30 dB were obtained when the active force was applied. For cases where these positions were different, reduction values varied from 6 to 13 dB.

All of the results obtained in this work came from simulations, however there is strong indication from the obtained results that this concept is applicable to real situations. A couple of adversities that would need to be overcome for this application are the selection of an actuator that presents the fast required response, which is a characteristic of the obtained optimal active forces, and the need of a fast detection system, which is able to quickly determine when there is contact between the sphere and plate, which indicates that an impact is occurring.

6.1 Future work

There are many interesting continuation possibilities from this work. The first step to take would be to correlate both the active and the impact force. As the impact force is dependent on the displacement of the top surface of the plate and the active force affects this displacement, the active force directly influences the time signature of the impact force. Thus, it is important to evaluate exactly how this influence develops. For this, a larger iterative loop could be used, repeating the whole process described in this work but maintaining the optimal active force found after the simulation and using it to evaluate a new impact force for each loop.

Another interesting next step is the addition of the acceleration noise to the simulations. As mentioned in section 2.1, this work focused solely on ringing noise, which makes up roughly half of the impact noise. Therefore, it is also important to

consider the acceleration noise. One possibility to do this is to add a dipole source that models the behavior of the acceleration noise and adding the influence from this dipole to the Reyleigh integral performed before the LMS algorithm.

One other improvement that could be done to the program is to add the possibility of consecutive impacts, as seen in real cases. The major difference being the fact that the plate will not be at rest for the impacts other than the first one. Also, there would be a certain inertia to the plate that would need to be evaluated for subsequent impacts. Adding this complexity to the simulation would allow for the study of cases more similar to real scenarios.

Lastly, an experiment should be set up to evaluate the applicability of the active force as proposed in this work. With the results of the experiment, an analysis of the coupling of the results between the simulation and the measurements would be possible. These would allow for an evaluation of the proposed methodology and the appropriateness of the concept of control of impact noise by means of an external force.

Bibliography

[1] Troccaz P, Woodcock R, Laville F. Acoustic radiation due to the inelastic impact of a sphere on a rectangular plate. J Acoust Soc Am, 2000;108(5):2197–2202.

[2] Nyström E. Controlling a one degree of motion impact. Chalmers Tekniska Högskola; 2013.

[3] Hoever C. Active structural control of impacts with a view towards noise control. Technische Universität Berlin; 2008.

[4] Micallef C. Active control of impact noise. Chalmers University of Technology; 2003.

[5] Kleiner M. Acoustics and Audio Technology. J. Ross Publishing; 2011 Oct 15.

[6] EN ISO 11688, Acoustics – Recommended practice for the design of low-noise machinery and equipment, Part 1: Planning; 1995

[7] Johnson KL. Contact mechanics. Cambridge university press; 1987 Aug 28.

[8] Rossing T.D., SpringerLink (e-book collection). Springer handbook of acoustics. New York, N.Y: Springer; 2007.

[9] Richards E.J., Westcott M.E., and Jeyapalan R.K.. On the prediction of impact noise, I: Acceleration noise. Journal of Sound Vibration, 62:547-575, February 1979.

[10] Silva C.W., editor. Vibration and Shock Handbook. Taylor & Francis Group, 2005.

[11] Jay L.O. and Negrut D.. Extensions of the HHT- method to dierential-algebraic equations in mechanics. Electronic Transactions on Numerical Analysis, 26:190-208, 2007.

[12] Siauw T., Bayen A.M., ScienceDirect (e-book collection). An introduction to MATLAB programming and numerical methods for engineers. Amsterdam: Academic Press, an imprint of Elsevier; 2015;2014;.

[13] Nelson P. A., Elliot S. J., Active Control of Sound, Academic Press (1992).

[14] Fuller C.R.. Active control of sound transmission/radiation from elastic plates by vibration inputs: I. Analysis. Journal of Sound and Vibration. 1990; 136(1):1-15.

[15] Metcalf V.L., Fuller C.R., Silcox R.J., Brown D.E.. Active control of sound transmission/radiation from elastic plates by vibration inputs, II: Experiments. Journal of Sound and Vibration. 1992; 153(3):387-402.

[16] Kropp W, Larsson K. Force estimation in the time domain by applying an LMS algorithm. Proc NOVEM 05; 18 April 2005; Saint-Raphaël, France 2005.

[17] Amiryarahmadi N, Kropp W, Larsson K. Application of LMS algorithm to measure low-frequency transient forces from human walking. Acta Acoustica united with Acustica. 2016;102(1):23-34.
[18] Popov V. Contact mechanics and friction: physical principles and applications. Springer Science & Business Media; 2010 Mar 10.
[19] Cremer L, Heckl M. Structure-borne sound: structural vibrations and sound radiation at audio frequencies. Springer Science & Business Media; 2013 Jun 29.
[20] Tornambe A. Modelling and controlling one-degree-of-freedom impacts under elastic/plastic deformations. InControl Theory and Applications, IEE Proceedings- 1996 Sep (Vol. 143, No. 5, pp. 470-476). IET.
[21] Nelson PA, Elliott SJ. Active control of sound. Academic press; 1991.